

Contents lists available at ScienceDirect

Earth-Science Reviews

journal homepage: www.elsevier.com/locate/earscirev





Contrasting characteristics, changes, and linkages of permafrost between the Arctic and the Third Pole

Xuejia Wang ^a, Youhua Ran ^{b,*}, Guojin Pang ^c, Deliang Chen ^{d,*}, Bo Su ^e, Rui Chen ^{f,g}, Xin Li ^{h,i}, Hans W. Chen ^j, Meixue Yang ^b, Xiaohua Gou ^a, M. Torre Jorgenson ^k, Juha Aalto ^l, Ren Li ^b, Xiaoqing Peng ^a, Tonghua Wu ^b, Gary D. Clow ^m, Guoning Wan ^b, Xiaodong Wu ^b, Dongliang Luo ^b

- ^a Key Laboratory of Western China's Environmental Systems (Ministry of Education), College of Earth and Environmental Sciences, Lanzhou University, Lanzhou 730000, China
- b Northwest Institute of Eco-Environment and Resources, Chinese Academy of Sciences, Lanzhou 730000, China
- ^c Faculty of Geomatics, Lanzhou Jiaotong University, Lanzhou 730070, China
- d Regional Climate Group, Department of Earth Sciences, University of Gothenburg, Gothenburg 40530, Sweden
- ^e State Key Laboratory of Earth Surface Processes and Resource Ecology, Beijing Normal University, Beijing 100875, China
- f Alfred Wegener Institute, Helmholtz Centre for Polar and Marine Research, Potsdam 14473, Germany
- g Geography Department, Humboldt University of Berlin, Berlin 10099, Germany
- h National Tibetan Plateau Data Center, Institute of Tibetan Plateau Research, Chinese Academy of Sciences, Beijing 100101, China
- ¹ CAS Center for Excellence in Tibetan Plateau Earth Sciences, Chinese Academy of Sciences, Beijing 100101, China
- ^j Department of Physical Geography and Ecosystem Science, Lund University, Lund 22362, Sweden
- ^k Alaska Ecoscience, Fairbanks, AK 99709, USA
- ¹ Department of Geosciences and Geography, University of Helsinki, Helsinki, Finland
- m Institute of Arctic and Alpine Research, University of Colorado, Boulder, CO 80309, USA

ARTICLE INFO

Keywords:
Permafrost degradation
Arctic
Third Pole
Tibetan Plateau
Climate warming
Active-layer thickness
Mean annual ground temperature
Geobazard

ABSTRACT

Permafrost degradation poses serious threats to both natural and human systems through its influence on ecological-hydrological processes, infrastructure stability, and the climate system. The Arctic and the Third Pole (Tibetan Plateau, TP hereafter) are the two northern regions on Earth with the most extensive permafrost areas. However, there is a lack of systematic comparisons of permafrost characteristics and its climate and ecoenvironment between these two regions and their susceptibility to disturbances. This study provides a comprehensive review of the climate, ecosystem characteristics, ground temperature, permafrost extent, and active-layer thickness, as well as the past and future changes in permafrost in the Arctic and the TP. The potential consequences associated with permafrost degradation are also examined. Lastly, possible connections between the two regions through land-ocean-atmosphere interactions are explored. Both regions have experienced dramatic warming in recent decades, characterized by Arctic amplification and elevation-dependent warming on the TP. Permafrost temperatures have increased more rapidly in the Arctic than on the TP, and will likely be reinforced under a future high emission scenario. Near-surface permafrost extents are projected to shrink in both regions in the coming decades, with a more dramatic decline in the TP. The active layer on the TP is thicker and has substantially deepened, and is projected to thicken more than in the Arctic. Widespread permafrost degradation increases geohazard risk and has already wielded considerable effects on the human and natural systems. Permafrost changes have also exerted a pronounced impact on the climate system through changes in permafrost carbon and land-atmosphere interactions. Future research should involve comparative studies of permafrost dynamics in both regions that integrate long-term observations, high-resolution satellite measurements, and advanced Earth System models, with emphasis on linkages between the two regions.

E-mail addresses: ranyh@lzb.ac.cn (Y. Ran), deliang@gvc.gu.se (D. Chen), deliang@gvc.gu.se (D. Luo).

^{*} Corresponding authors.

1. Introduction

Permafrost is an "invisible" (subsurface) component of the cryosphere defined as ground (soil or rock and included ice or organic material) that remains at or below 0 °C for at least two consecutive years (Dobinski, 2011). Permafrost occupies between 14 and 16×10^6 km² of the Earth's exposed land surface. It covers some 15% of the exposed land area of the Northern Hemisphere (NH) (Obu, 2021; Ran et al., 2022), and is distributed primarily in the Arctic and in mid-latitude mountainous regions (Fig. 1). One such region is the Tibetan Plateau (TP), which is often referred to as the "Third Pole" owing to its largest storage of ice masses on Earth outside the Arctic and Antarctic regions (Yao et al., 2019). Although permafrost domains are not densely populated, their economic importance has grown because of their abundant natural resources (Nelson et al., 2002). The thermal state of permafrost can be highly susceptible to disturbance such as changes in air temperature and ecosystem properties, consequences of both natural and human factors (Park et al., 2016). Permafrost can persist in areas where the mean annual air temperature (MAAT) is as high as +2 °C, or degrade in areas where the MAAT is around -20 °C (Jorgenson et al., 2010; Ran et al., 2022). In concert with the unprecedented climate warming (IPCC, 2021), global permafrost temperatures have increased significantly (Biskaborn et al., 2019), leading to permafrost degradation that exerts large impacts on climatological and ecological-hydrological processes through interactions between the Earth's spheres (Yang et al., 2010; Koven et al., 2011; Schaefer et al., 2014; Schuur et al., 2015; Hjort et al., 2018; Teufel and Sushama, 2019).

Permafrost degradation has large impacts on processes from global to local-scales. As a large carbon reservoir, permafrost holds about half of all the terrestrial storage, equivalent to nearly twice as much carbon as the atmosphere (Schuur et al., 2008; Hugelius et al., 2014; Schuur et al., 2015). Carbon release caused by permafrost warming through oxidation of organic matter may therefore accelerate climate warming (Schuur et al., 2015). Permafrost also contains large amounts of ground ice, and the areas with ice content are found at high latitudes and in high plateaus and mountains (Zhang et al., 1999). If subsurface ice in permafrost regions undergoes large-scale melting, it has a potential for substantial effects on critical infrastructure, landscapes, hydrology, and water resources (Zhang et al., 1999; Cheng and Wu, 2007; Rennermalm

et al., 2010). Permafrost forms an impermeable layer and prevents penetration of precipitation or snowmelt water, inducing high moisture levels in the active layer (Hinzman et al., 2005). Hydrological activity is generally limited to the active layer, which provides moisture to the biosphere and atmosphere. Once permafrost thaws, the impermeable layer is damaged and hydrological activities and cascading physical processes can be modified substantially (Cheng and Wu, 2007; Gruber et al., 2017; IPCC, 2019; Song et al., 2019). To better predict and mitigate these effects, an in-depth understanding of the current status of permafrost in high-latitude and high-altitude areas, and the response of permafrost to the unprecedented climate change under different environmental conditions are crucially needed.

The Arctic has warmed more rapidly and drastically than the global average since the mid-20th century, a phenomenon known as Arctic amplification (AA) (Serreze and Barry, 2011). Changes in the surface temperatures of the Arctic have been amplified through snow/sea-ice albedo feedback and other physical processes (Cohen et al., 2018). Near-surface air temperatures over the Arctic region have risen dramatically, at a rate 2–3 times the global average (Cohen et al., 2014; Huang et al., 2017). The Arctic cryosphere is an important component of the Earth system and has a significant influence on the Earth's energy budget, atmospheric and ocean circulations, freshwater storage, sealevel rise, as well as the storage and release of large amounts of greenhouse gases, among other effects (Olsen et al., 2011). Partly driven by the AA, the hydrological cycle in the Arctic has intensified, and various components of the Arctic system have changed significantly (Box et al., 2019; Landrum and Holland, 2020), including active layer thickening, permafrost degradation, and settlement of the ground surface.

The TP has long been recognized to profoundly influence regional, Asian, and even global climate and weather systems through both dynamic and thermal forcing (Wu et al., 2014; Xu et al., 2021). The TP and adjacent mountain ranges have been referred to as the "Asian water tower" because several large river systems (e.g., the Yangtze, Yellow, Indus, and the Mekong) originate in this region, providing a substantial portion of both natural and anthropogenic water demands (Immerzeel et al., 2020). The TP is arguably the world's most important and vulnerable water tower component (Immerzeel et al., 2020) because it is more responsive to the radiative forcing of greenhouse gases and snow albedo than other areas in the same latitudes (You et al., 2020). The TP

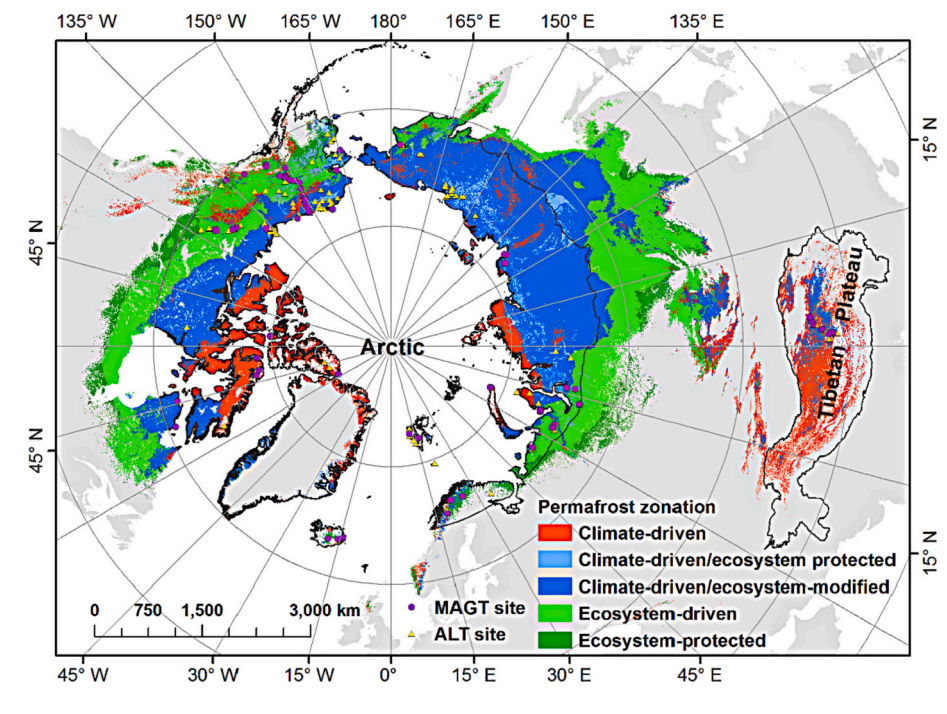


Fig. 1. Biophysical permafrost zonation in the Arctic and the Tibetan Plateau (TP), also known as the Third Pole, during 2000-2016 (source: Ran et al., 2021b). The boundaries of the Arctic and TP are the same as in Li et al. (2020). The Arctic mainly refers to the geographical region north of the Arctic Circle (66°32'N) together with the land areas northward of 62°N in Asia and 60°N in North America, and modified to contain the marine areas north of the Aleutian chain, Hudson Bay, and parts of the North Atlantic Ocean including the Labrador Sea (AMAP, 1997). The Arctic is further divided into three subregions: Greenland, Eurasia, and North America. In this study, only the land parts are considered. The TP is defined as the areas around the plateau with elevations equal to or above 4000 m, covering the Qinghai-Tibetan Plateau, Hengduan Mountains, the Himalayas, the Hindu Kush, and the Pamir Plateau (Liu et al., 2014a). Mean annual ground temperature (MAGT) sites used in the study are selected from the Global Terrestrial Network for Permafrost (GTN-P) (Biskaborn et al., 2019). Active-layer thickness (ALT) sites in the TP are same as the study of Li et al. (2012a).

possesses the largest amount of permafrost in the mid-and low-latitude regions and is the dominant high-altitude permafrost region in the NH, accounting for the great majority of permafrost in China (Ran et al., 2012). Along with the dramatic climate warming since the 1960s, direct evidence has revealed significant losses of the TP cryosphere including glaciers, frozen ground, and snow cover (Ran et al., 2018; Yang et al., 2019).

The current distributions of permafrost and ground ice are the result of the historical evolution of permafrost during the Last Glacial Maximum or Last Permafrost Maximum, as well as recent climate and heat exchange conditions between the land surface and the atmosphere (Zhang et al., 1999; Jin et al., 2019; Zhao et al., 2020). Between the Arctic and the TP, there are divergent effects of Pleistocene glacial development on permafrost. In general, the permafrost history of the TP is shorter than that of the Arctic (Cheng, 1979), forming different degrees of ecosystem fragility. Besides the above aspects, local disturbances modulate the variations of permafrost as well. Snow, vegetation, soil properties (e.g., soil type, soil organic matter content, and soil moisture), and topographically-influenced factors (e.g., solar radiation and hydrology) regulate the heat and water exchanges between land and the atmosphere, leading to complex processes controlling the ground thermal regime (Karjalainen et al., 2019a, 2019b; Jiang et al., 2020). The vegetation distributions and dynamics in the Arctic and TP are different, which exerts a marked influence on permafrost evolution through the main driver of Earth's energy and water budgets, i.e., land surface-atmosphere interactions (Cheng, 1979; Shur and Jorgenson,

The Arctic and the TP are both extremely sensitive to global climate change and can act as indicators for changes because both have shown amplified warming under global warming (You et al., 2021). Previous studies suggested that the two regions have varying feedbacks and responses to global change with shared linkages (e.g., Cohen et al., 2018; Wang et al., 2018a; Gao et al., 2019; Qian et al., 2019; You et al., 2021). Yet, significant differences between the Arctic and the TP cause permafrost to exhibit disparate responses to climate change and human activities. To date, the mechanisms and interconnections between the two regions remain inconclusive, as most permafrost studies have focused exclusively on one or the other of the two regions and there have not been many attempts to systematically contrast the permafrost characteristics between them. A systematic study incorporating the two regions plays a vital role in global change research (Guo et al., 2020). It is therefore important to comprehensively compare permafrost characteristics and its formative environment, and discuss possible connections between the two polar regions.

The objectives of this paper are to: (1) compare the climate and ecosystem characteristics between the Arctic and the TP; (2) summarize similarities and differences in permafrost characteristics between the two regions, in terms of near-surface permafrost distribution, permafrost temperature, active-layer thickness (ALT), ground ice, and permafrost carbon storage; (3) assess the historical and future trajectory of permafrost in the two regions in the context of human-induced climate change; (4) evaluate the risks and potential impacts of permafrost degradation on socio-ecological systems; and (5) highlight possible connections between the Arctic and TP. Finally, we will conclude with some potentially important future developments for research.

2. Climate and ecosystem characteristics

Interactions involving climatic and ecological processes during permafrost formation and degradation are complex. There are negative departures in air temperature from the long-term averages in both regions, especially in winter, facilitating permafrost development. Air temperatures in the Arctic are much colder than on the TP, especially over Greenland, Siberia, and northern Canada, owing to the high latitude, weak solar radiation, and high reflectance and insulation effect of polar sea ice. Thus, the Arctic has a larger freezing index and a smaller

thawing index (Table 1). Compared with the TP, most of the Arctic experiences larger annual temperature ranges and slightly greater annual precipitation, with the exception of parts of North America and Greenland. Snow depth and snow cover duration also are appreciably greater in the Arctic, and vegetation greenness as indicated by the leaf area index is higher.

In general, ecosystems play an important role in permafrost development. In continuous permafrost zones, ecosystem properties, such as vegetation succession and organic matter accumulation, result in the formation of an ice-rich layer at the top of permafrost (Shur et al., 2005). In the subarctic, ecosystems—through the interaction of biophysical factors with soil temperature—can also create conditions leading to the preservation and formation of discontinuous permafrost under poorly drained, low-lying, and north-facing landscape conditions. Farther south in the subarctic, ecosystem-protected permafrost persists in the form of sporadic patches under warmer climatic conditions (Shur and Jorgenson, 2007). The markedly different vegetation distributions in the Arctic and TP can result in a thicker active layer on the TP than in much of the Arctic when other conditions are the same (Cheng, 1979). Boreal forests and mosses cover large areas of the Russian, Canadian, and Alaska permafrost areas, in contrast to the permafrost areas on the TP where no trees exist, and vegetation is dominated by perennial herbaceous plants. Moreover, shrub expansion is occurring in many tundra ecosystems and has been linked to "greening" across the Arctic (Tape et al., 2006; Myers-Smith et al., 2011). For the TP, vegetation cover is one of the most important factors that affect permafrost through modified soil hydrothermal regimes (Wang et al., 2012). The TP vegetation greening is dominated by the main vegetation types, including grassland, shrubland, and meadow (Pang et al., 2017; Li et al., 2018). These ecosystem shifts will evoke a significant response of permafrost evolution via altered atmosphere-surface interactions (Shur and Jorgenson, 2007; Ran et al., 2021b; Heijmans et al., 2022).

The NH land-surface MAAT has risen strikingly, on average by 0.3 $^{\circ}\text{C}$ decade⁻¹, over the period 1979–2018 (Fig. 2). For the Arctic land area, the air temperature increase has outpaced the global and NH mean temperature increases, at a rate of up to 0.5 °C decade⁻¹ over the same period. A previous study has revealed that Arctic warming is evident and is occurring in all seasons, but is strongest over the Arctic in autumn and winter and weakest in summer (Table 1; Cohen et al., 2018). The vertical distribution of Arctic air temperatures indicates that the warming extends almost through the entire troposphere but is concentrated near the land surface (Perlwitz et al., 2015). A newly constructed Arctic surface air temperature dataset suggests that warming in the Arctic (including areas of the ocean) reached 0.8 °C decade⁻¹ over the period 1998–2012 (Huang et al., 2017). Based on an analysis of a new 31 station data set, enhanced climate warming has also been reported in the Alaskan Arctic during 1998-2015 (Wang et al., 2017). These updated estimates of Arctic warming largely contribute to a continual global and NH warming, contrary to the controversial warming hiatus or slowdown during 1998-2012.

Compared with the NH (including land and ocean), warming of the TP began earlier and has been more pronounced (Yao et al., 2019). The TP has witnessed dramatic warming since the 1960s, at a rate of 0.3–0.4 °C decade⁻¹ (Chen et al., 2015), and since 1979 MAAT has increased 0.3 °C decade⁻¹ (Fig. 2). The warming is apparent across all seasons, with the strongest warming occurring in spring and the weakest in summer for the period 1979–2018 (Table 1). Elevation-dependent warming, in which greater warming is more likely to occur at higher elevations, is evident on the TP (Rangwala et al., 2009; Pepin et al., 2015; You et al., 2020). Elevation-dependent warming can accelerate the rate of change in the climate system, because the mechanisms associated with e.g. snow-albedo and water vapor-radiative feedbacks, generate greater warming response at higher elevations (Pepin et al., 2015). This is a special characteristic of the TP climate warming due to the absence of extensive mountain ranges in the Arctic.

Under future emission scenarios, air temperature increases in the

Table 1

The climate and ecosystem characteristics in the permafrost zones of the Arctic and TP. Freezing (thawing) index is calculated as the sum of the daily temperatures for all days below (above) 0 °C temperatures during the freezing (thawing) period (Frauenfeld et al., 2007), in which the freezing period is defined to be from July to June of the following year, and a thawing period of January to December. An asterisk (*) indicates that the trend is significant at the 95% confidence level.

Variable	Spatial mean and standard deviation (mean $\pm\sigma)$					Data source
	Arctic	Arctic subregions			TP	
		Eurasia	North America	Greenland		
Mean annual air temperature (°C)	-12.4 ± 6.4	-10.9 ± 4.2	-10.0 ± 5.8	-19.0 ± 6.4	-4.7 ± 4.4	WorldClim v2 for 1970–2000; Fick and Hijmans, 2017
Freezing index (°C)	4922.6 ± 164.0	$4910.8 \pm \\226.9$	$\begin{array}{c} \textbf{4454.1} \; \pm \\ \textbf{234.7} \end{array}$	6391.1 ± 274.4	838.3 ± 94.5	CRUNCEP v8 daily air temperature for 1979–2008; Viovy, 2018
Thawing index (°C)	522.1 ± 47.6	948.7 ± 72.5	696.9 ± 62.6	$\textbf{0.0} \pm \textbf{0.0}$	1759.9 ± 77.0	CRUNCEP v8 daily air temperature for 1979–2008; Viovy, 2018
Air temperature annual range (°C)	36.1 ± 9.9	40.5 ± 10.6	36.6 ± 6.4	26.1 ± 5.6	23.5 ± 3.1	WorldClim v2 for 1970–2000; Fick and Hijmans, 2017
Air temperature trend (°C decade ⁻¹)	DJF: 0.58* MAM: 0.52* JJA: 0.33* SON: 0.60*	-	-	-	DJF: 0.29* MAM: 0.35* JJA: 0.23* SON: 0.24*	CRU TS4.02 data for 1979–2018; Mitchell and Jones, 2005
Annual precipitation (mm)	363.5 ± 239.6	$\begin{array}{c} \textbf{346.2} \pm \\ \textbf{161.3} \end{array}$	291.7 ± 93.4	527.4 \pm 347.1	$\begin{array}{c} \textbf{298.3} \pm \\ \textbf{206.2} \end{array}$	WorldClim v2 for 1970–2000; Fick and Hijmans, 2017
Precipitation trend/ mm decade ⁻¹	DJF: 1.00 MAM: 0.76 JJA: 0.69 SON: 2.36*	-	-	-	DJF: -0.72 MAM: 1.97 JJA: 2.52 SON: -0.28	CRU TS4.02 data for 1979–2018; Mitchell and Jones, 2005
Snow depth (cm)	26.0 ± 10.1	27.6 ± 10.9	24.2 ± 8.9	_	2.4 ± 2.9	Takala et al., 2011; Che et al., 2008
Snow cover duration (days)	267.8 ± 36.5	245.3 ± 22.9	253.1 ± 33.0	338.4 ± 19.8	$\textbf{75.9} \pm \textbf{66.4}$	Hori et al., 2017
Leaf area index	0.45 ± 0.31	0.47 ± 0.26	0.38 ± 0.36	_	0.19 ± 0.27	GLASS LAI product; Xiao et al., 2014
Soil organic carbon content (g kg ⁻¹)	121.8 ± 55.6	126.7 ± 61.7	113.1 ± 44.1	154.4 ± 62.1	29.8 ± 24.8	SoilGrid250; Hengl et al., 2017
Ground ice (×10 ³ km ³)	11.39–26.42	7.00–14.90	4.38–11.19	0.33	12.70	Brown et al., 2002; Zhao et al., 2019; Cheng et al., 2019

DJF: December–February, MAM: March–May, JJA: June–August, SON: September–November.

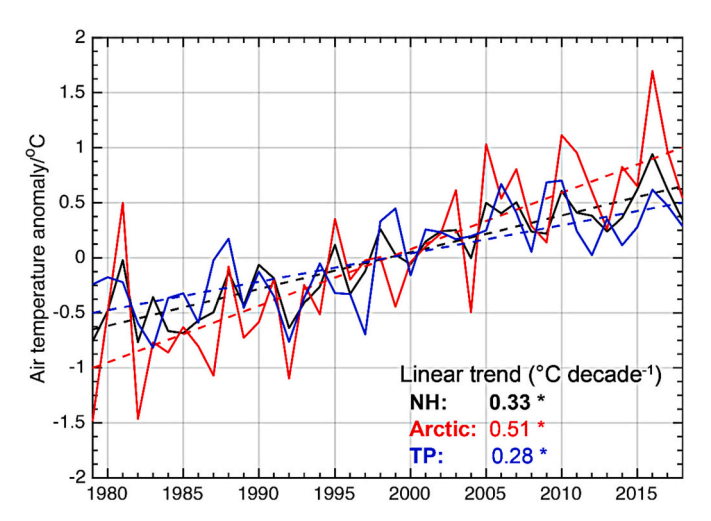


Fig. 2. Changes in mean annual land-surface air temperature anomaly (relative to 1979–2018 mean annual temperature) over the Northern Hemisphere (NH; black), Arctic ($60^{\circ}N-90^{\circ}N$; red), and the Third Pole (TP; blue) between 1979 and 2018 based on the Climate Research Unit (CRU) TS4.02 data (Mitchell and Jones, 2005) at a spatial resolution of 0.5° . Dashed lines are linear regression lines. The trends shown in the panel are based on the linear regression. An asterisk (*) indicates that the trend is significant at the 95% confidence level. (For interpretation of the references to colour in this figure legend, the reader is referred to the web version of this article.)

Arctic and TP are projected to continue for the remainder of the 21st century. The temperature increases of the high-latitude permafrost (referred to as circumpolar permafrost) regions are predicted to be generally greater than those in high-altitude permafrost (mountain permafrost) regions (Guo et al., 2018). The Coupled Model

Intercomparison Project Phase 5 (CMIP5) models have projected that the ensemble MAAT will increase by 3.8 °C and 8.0 °C by 2099 over the high-latitude permafrost areas in the Representative Concentration Pathway (RCP) 4.5 and RCP 8.5 scenarios, respectively; the corresponding projected ensemble MAAT increases over the high-altitude permafrost areas, including the TP, are smaller with 2.9 °C for RCP 4.5 and 6.0 °C for RCP 8.5 (Guo and Wang, 2016). The new generation CMIP6 models have projected that MAAT will exceed 0 °C throughout the northwestern Siberia during 2071–2100 under the SSP5–8.5 scenario (Alexandrov et al., 2021). These projections suggest that air temperatures would rise more rapidly over the Arctic permafrost area than the TP permafrost area.

3. Current permafrost characteristics

3.1. Permafrost extent

To discuss permafrost extent, we must distinguish two concepts: area of a permafrost region and permafrost area. In the former, the regions may not be underlain by permafrost in their entirety; the notion of permafrost region is beneficial for cartography, studying soil properties, plant ecology, hydrological pathways, and civil engineering (Obu, 2021). The latter is the actual permafrost area underlain by permafrost (Zhang et al., 2000; Gruber, 2012; Obu et al., 2019). Their differences are mainly related to mapping scale and study purposes (Nelson et al., 2002; Ran et al., 2012). The permafrost area is essentially smaller than the area of a permafrost region because permafrost only underlies a portion of the permafrost region (Gruber, 2012; Heginbottom et al., 2012). Various classification systems have been used to describe the types of permafrost region. Areal continuity-based systems are popularly used. According to the areal continuity, the permafrost region in the Arctic occupies two commonly depicted latitudinal zones, continuous (>90% of the area) and discontinuous (50–90% of the area) permafrost,

while the TP is dominated by discontinuous and sporadic (10-50% of the area) permafrost (Brown et al., 2002). The areal continuity-based systems are useful to characterize permafrost distribution in highlatitude areas for differentiating climatic influence, but fail to explicitly identify the role of ecosystem properties in the formation and evolution of permafrost (Shur and Jorgenson, 2007; Ran et al., 2021b). Such systems are also highly controversial for describing permafrost distribution on the TP due to their ambiguous definition and scaledependency (Cheng, 1984; Ran et al., 2012, 2018, 2021a). Recent mapping efforts have adopted a biophysical zonation, by using a rulebased GIS model that integrates global climate and ecological datasets, to classify the NH permafrost regions into climate-driven, climatedriven/ecosystem-modified, climate-driven/ecosystem ecosystem-driven, and ecosystem-protected subregions (Ran et al., 2021b). This provides a new perspective to describe the complex interactions of climatic and ecological processes with permafrost. The new map shows that both the Arctic and the TP are dominated by climatedriven and climate-driven/ecosystem-modified permafrost (Ran et al., 2021b; Fig.1). However, the hydrothermal conditions of permafrost are very different between the Arctic and TP, the cold-humid permafrost generally dominates in the High Arctic while the warm-arid type dominates in the TP (Ran et al., 2022).

According to the International Permafrost Association (IPA) map, the calculated area included in permafrost regions is $10.85\times10^6~\mathrm{km}^2$ in the Arctic and $1.88\times10^6~\mathrm{km}^2$ on the TP (Table 2) while the corresponding values of permafrost area, defined as the area of permafrost region multiplied by the fraction of areal continuity (Zhang et al., 2000), are $9.53\times10^6~\mathrm{km}^2$ and $0.96\times10^6~\mathrm{km}^2$, respectively. Several permafrost maps have been compiled to evaluate the distribution and thermal states of the permafrost in the Arctic and on the TP (Table 2). The estimated permafrost area in the Arctic during 2000–2014 is $9.78\times10^6~\mathrm{km}^2$ based on a threshold of 0 °C mean annual ground temperature (MAGT) at the depth of zero annual amplitude (DZAA) (Karjalainen et al., 2019b). On

Table 2 Permafrost area in the Arctic and the TP (unit: 10⁶ km²).

Area of permafrost region		Permafrost area		Method and reference
Arctic	TP	Arctic	TP	
10.85	1.88	9.53	0.96	IPA permafrost zonation map, compiled by Brown et al. (2002) based on national and regional maps and expert knowledge from different sources and time periods. The areas of permafrost were derived from permafrost regions, which are defined as the area of permafrost region multiplied by areal continuity fraction (Zhang et al., 2000).
11.75	1.74	9.50	1.34	Permafrost zonation based on modeled permafrost probabilities for 2000–2016 using the TTOP model (Obu et al., 2019).
-	-	9.55	1.29	Derived from mean annual ground temperature (≤ 0 °C) at the top of the permafrost for 2000–2016 estimated by Obu et al. (2019) using the TTOP model.
-	-	9.78	1.17	Derived from mean annual ground temperature (≤ 0 °C) for 2000–2014 estimated by Karjalainen et al. (2019b) based on downscaled climate data and updated for the TP using the method in Ran et al. (2021a).
-	-	-	1.37	Derived from mean annual ground temperature $(\le 0 \text{ °C})$ for 2005–2015 estimated by Ran et al. (2021a) based on remote sensed data and adjusted for the new boundary of the TP shown in Fig. 1.
10.68	1.46	10.11	1.18	Derived from mean annual ground temperature (\leq 0 °C) for the period of 2000–2016 estimated by Ran et al. (2022), which integrates a large amount of field measurement and remote sensed data using machine learning techniques.

the TP, the permafrost area is estimated to be $1.37 \times 10^6 \text{ km}^2$, accounting for 34% of the TP area, based on machine learning, satellite data, and site measurements from 2000 to 2016 (Ran et al., 2021a). New permafrost area estimates at a 1-km scale based on the threshold MAGT $<\!0$ °C are 10.11 \times 10^6 km² in the Arctic and 1.18 \times 10^6 km² on the TP (Fig. 1; Ran et al., 2021b, 2022). Several other permafrost maps have also reported the TP permafrost area (Li and Cheng, 1996; Zou et al., 2017; Obu et al., 2019; Ni et al., 2021; Ran et al., 2021a), which differ significantly due to varying data collection periods, mapping methods, and regional boundaries for statistics, as well as limited data sources. In addition, permafrost modeling and permafrost area calculations are unavoidably affected by uncertainties associated with data limitations, mathematical methods, underlying assumptions for the calculations, and parameterization schemes, which call for estimating the uncertainty range according to multiple calculated values of the permafrost area considering different scenarios.

3.2. Ground temperature and active-layer thickness

Ground temperature and ALT are the most commonly used indicators of permafrost characteristics and thermal state. Permafrost thickness can vary between the Arctic and TP due to the different historical evolution of permafrost. Areas at the southern limit of permafrost distribution of the Arctic, such as Siberia, with permafrost thicknesses of 250-300 m under a MAGT of about -5 °C, supported a small-scale ice cap during the Pleistocene era, while Canada, with permafrost thicknesses of 60-100 m, experienced 97% coverage by glaciers (Cheng, 1979; Turner and Schuster, 1996; Bosikov, 1998). In Arctic Alaska, where the MAGT ranged from -10 to -12 °C before the 1990s (Lachenbruch and Marshall, 1986), permafrost thicknesses range from 250 to 650 m, depending primarily on the thermophysical properties of the rock units (Lachenbruch et al., 1982; Clow, 2014). For the TP, the permafrost thickness is estimated to be 120-160 m in areas with a MAGT of around -5 °C, noticeably less than that of Siberia but greater than that of Canada, partially because no large ice sheet developed on the TP during the Quaternary era and late uplift period of this region (Cheng, 1979; Wang and French, 1995).

Permafrost temperatures in the Arctic rise along a north-south bioclimatic gradient, from $<-14\ ^{\circ}\text{C}$ in the Canadian High Arctic to <0 °C close to the southern limits of permafrost occurrence (Streletskiy et al., 2017). The average MAGT from 83 boreholes in the Arctic permafrost area from Biskaborn et al. (2019) was -3.4 °C for a recent decade (2007-2016) (Fig. 3). Based on a statistical modeling approach (Aalto et al., 2018), the average MAGT across the entire Arctic permafrost area was -5.9 ± 3.5 °C from 2000 to 2014. On the TP, MAGT recorded by 12 boreholes from 2007 to 2016 ranged from -3.0 to -0.1 °C and decreased gradually with increasing altitude, with an overall MAGT of -1.9 ± 1.8 °C in the permafrost area from 2000 to 2014 (Table 3). This comparison indicates that the Arctic permafrost should be regarded as "cold permafrost", while the TP permafrost should be classified as "warm permafrost". Based on MAGT, permafrost can be characterized as sub-stable (-3 $^{\circ}\text{C} < \text{MAGT} < -1.5$ $^{\circ}\text{C}),$ transitional (-1.5 $^{\circ}\text{C}$ < MAGT < -0.5 $^{\circ}\text{C}$), and unstable permafrost (-0.5 $^{\circ}\text{C}$ < MAGT <0.5 °C) (Cheng and Wang, 1982), which together account for 75.1% of the TP permafrost area (Zhao et al., 2020).

Overlying permafrost is the active layer, which thaws in summer and refreezes in winter. The ALT ranges from <50 cm in northern Alaska and Siberia to >300 cm on the TP (Luo et al., 2016; Peng et al., 2018). According to more than 230 sites from the Circumpolar Active Layer Monitoring (CALM) network, the mean ALT across sites and years was 48 cm in Alaska, 93 cm in Canada, and 74 cm in Russia from 1990 to 2015 (Luo et al., 2016), while the mean ALT for 142 sites in the Arctic was 68 cm. Based on the Stefan solution considering the thawing index and edaphic factor (Peng et al., 2018), we estimated that the regional average ALT was 100 cm in the Arctic during 2000–2014, 104 cm in Eurasia, 98 cm in North America, and 50 cm in Greenland (Table 3).

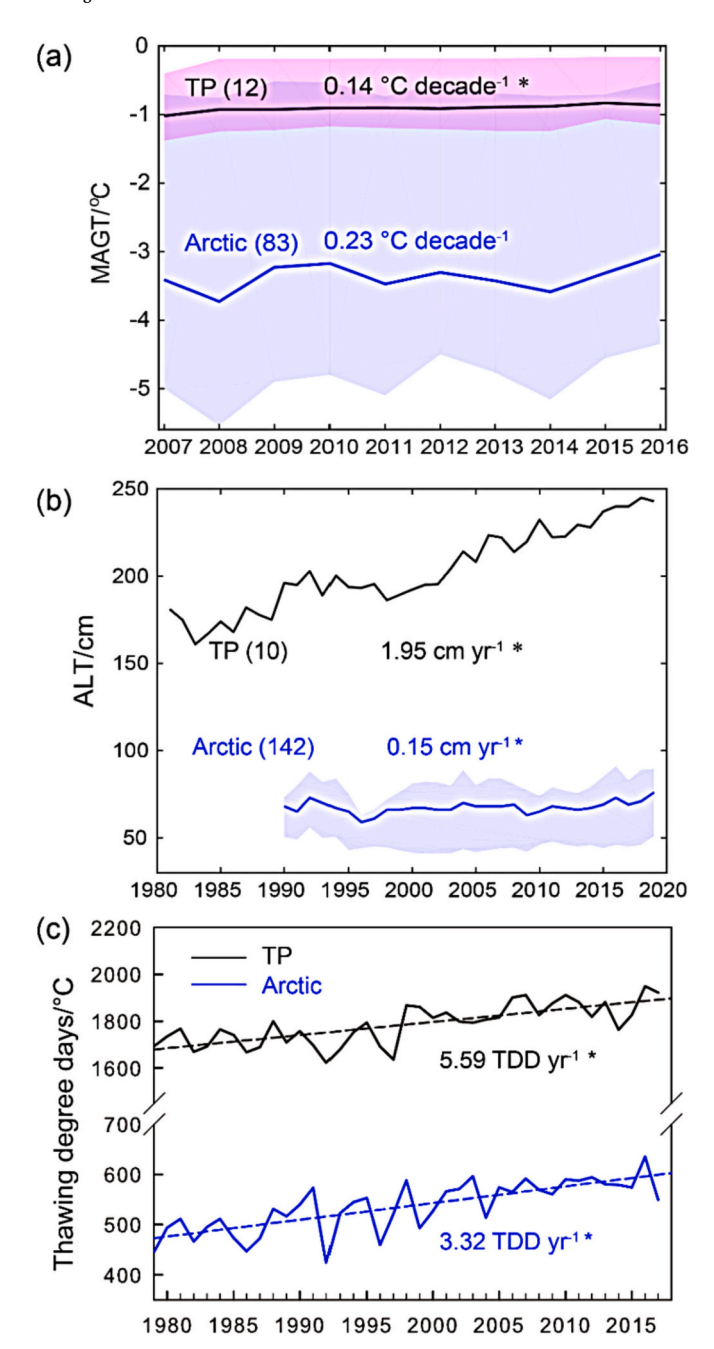


Fig. 3. Changes in (a) mean annual ground temperature (MAGT) (°C), (b) active-layer thickness (ALT) (cm), and (c) thawing degree days (TDD) (°C) in the Arctic and TP over the past decades. The shading in (a) denotes the 25% and 75% percentiles of MAGT measured by borehole sites in the Arctic and TP from GTN-P (from Biskaborn et al., 2019). The ALT data in the Arctic were selected from the Circumpolar Active Layer Monitoring (CALM) Program Network, while the TP data were obtained from Li et al. (2012a). The number of sites used in the aggregation are shown in brackets. The trends shown in the panel are based on linear regressions. An asterisk (*) indicates that the trend is significant at the 95% confidence level. The thawing degree days were calculated based on daily air temperature of the CRUNCEP v8 dataset (Viovy, 2018). Compared to other bias-corrected reanalysis datasets, the CRUNCEP dataset stands out for ecosystem process simulation at the global scale (Wu et al., 2018).

Mean ALT along the Qinghai-Tibetan Highway (QTH) was 203 cm according to ground-based ALT measurements from 1982 to 2018. For the entire TP, ALT generally decreases with increasing elevation, ranging from 100 cm to more than 300 cm, with an average of 212 cm (Table 3).

This is slightly lower than the simulated ALT, found by a 1-D numerical heat diffusion model with phase change, $\sim\!230$ cm (221–240 cm) (Qin et al., 2017). Overall, ALT is two-fold higher within the TP than in the Arctic.

3.3. Ground ice

In general, ice-rich permafrost with a high ice content (> 20% by volume) and relatively thick overburden cover (> 5–10 m) occurs in the high latitudes, occupying approximately 8.6% of the total permafrost area, while ice-poor permafrost with a low ice content (< 10% by volume, with either thick or thin overburden cover) is mostly located in mountainous areas and high plateaus, occupying approximately 66.5% of the total permafrost area (Zhang et al., 1999). Based on alternative assumptions, approximately 11.37–36.55 \times 10 3 km 3 of ground ice may be stored in the NH permafrost, corresponding to an equivalent sea-level rise of 3–10 cm (Zhang et al., 1999). Following the method of Zhang et al. (1999), as well as the IPA permafrost map and ground-ice conditions (Brown et al., 2002), ground ice in the Arctic permafrost region has been estimated to be approximately 11.39–26.42 \times 10 3 km 3 (1.05–2.44 \times 10 $^{-3}$ km 3 per km 2), with largest values in Eurasia and North America.

On the TP, total ground ice storage within the permafrost regions is roughly 9.53×10^3 km³ (8.99×10^{-3} km³ per km²), based on the ground ice distribution in the different topographic units along the QTH (Zhao et al., 2010). Recent permafrost investigations and field-based studies reported the ground ice storage to be 12.7×10^3 km³ water-equivalent (Zhao et al., 2020). In the continuous permafrost area, ground-ice exhibits east-west and south-north increasing gradients in the TP, with two maximum centers in the Kunlun Mountains and Hoh Xil area (Cheng et al., 2019). In the source region of the Yellow River (covering an area of about 2.9×10^4 km² above Duoshixia) (Luo et al., 2011) on the northeastern TP, the total volume of ground ice at depths of 3–10 m is approximately 51.68 ± 18.81 km³ (Wang et al., 2018b).

3.4. Permafrost carbon storage

There is a growing concern about soil carbon storage in permafrost because it is of great significance for global warming (Schuur et al., 2008). When permafrost thaws, a significant amount of carbon stock in the permafrost layers could be subject to increased decomposition and release of trace gases. Soil organic carbon (SOC) stocks in the northern circumpolar permafrost are estimated to be approximately 1035 ± 150 Pg in the upper soil (0-3 m) (Hugelius et al., 2014), with an extra 648 Pg in the lower depths (3-25 m) (Tarnocai et al., 2009). According to the SoilGrids system at 250-m resolution (Hengl et al., 2017), SOC content in the Arctic has been estimated to be 121.82 g kg⁻¹, with Greenland having the largest value of 154.44 g kg⁻¹ (Table 1). SOC storage is generally associated with land cover type, ALT, soil moisture, soil texture, and pH value (Yang et al., 2008; Baumann et al., 2009; Elberling et al., 2013; Mu et al., 2015, 2020). The thick peat layers in the circumpolar permafrost with its abundant soil organic matter, however, also complicate soil carbon response due to the effects of soil thermal insulation on soil thermal and moisture regimes (Park et al., 2016). Because of the thermal and hydraulic properties of organic soils, SOC is another factor expected to affect permafrost active layer processes (Fisher et al., 2016; Zhu et al., 2019).

On the TP, the estimated SOC storage in the upper 1 m is 7.4 Pg in alpine grasslands (Yang et al., 2008). Using 190 soil profiles located in three typical vegetation-type areas—alpine steppe, alpine meadow, and alpine desert—the SOC has recently been estimated to be 33 Pg in the top 3 m and 127.2 Pg within 3–25 m. Stocks of 132 Pg out of the total 160 Pg SOC are in the permafrost layer, excluding the active layer (Mu et al., 2015). Through large-scale systematic field investigations of permafrost soil carbon, spatially explicit estimates of SOC indicate that 15.31 Pg is stored in the top 3 m of alpine grasslands (Ding et al., 2016). Based on SOC observations after 2006 in the TP permafrost region and

Table 3 Statistics of mean annual ground temperature (MAGT) (mean \pm σ °C) in the permafrost region, near-surface permafrost (< 10–15 m depth) area (PE, 10^6 km²), and active-layer thickness (ALT) (mean \pm σ cm) in the Arctic and the TP over three periods: baseline (2000–2014), 2041–2060, and 2061–2080 under the RCP 4.5 and RCP 8.5 scenarios. For the Arctic, data for MAGT and PE in the Arctic are from Aalto et al. (2018) and Karjalainen et al. (2019b), and data for ALT are based on the Stefan solution using the thawing index derived by the multi-model ensemble mean of CMIP5 GCMs and the edaphic factor (Peng et al., 2018). For the TP, the calculations in this study are the same as those for the Arctic, except that the atmospheric forcing data uses the downscaled climate data, i.e. WorldClim (Ran et al., 2022).

		Arctic	Arctic subregions	TP		
	<u> </u>		Eurasia	North America	Greenland	
MAGT						
Baseline	2000-2014	-5.9 ± 3.4	-5.5 ± 2.6	-6.1 ± 3.9	-8.5 ± 3.7	-1.9 ± 1.8
RCP 4.5	2041-2060	-2.8 ± 3.1	-2.3 ± 2.3	-3.2 ± 3.6	-5.8 ± 3.2	-0.4 ± 1.5
	2061-2080	-2.1 ± 3.0	-1.6 ± 2.3	-2.5 ± 3.4	-5.1 ± 3.0	0.0 ± 1.5
RCP 8.5	2041-2060	-2.1 ± 3.0	-1.5 ± 2.3	-2.5 ± 3.5	-5.1 ± 3.0	0.0 ± 1.5
	2061–2080	-0.5 ± 3.0	0.2 ± 2.3	-0.9 ± 3.4	-3.7 ± 2.8	1.0 ± 1.5
PE						
Baseline	2000-2014	9.78	5.21	4.32	0.25	1.17
RCP 4.5	2041-2060	7.60	4.19	3.18	0.23	0.64
	2061-2080	6.99	3.79	2.99	0.21	0.49
RCP 8.5	2041-2060	6.94	3.75	2.98	0.21	0.48
	2061–2080	4.97	2.41	2.38	0.18	0.19
ALT						
Baseline	2000-2014	100.18 ± 43.16	104.49 ± 33.67	98.21 ± 51.47	49.97 ± 32.52	212.03 ± 78.15
RCP 4.5	2041-2060	111.41 ± 46.55	115.76 ± 35.60	109.27 ± 56.49	62.81 ± 35.33	265.75 ± 82.11
	2061-2080	114.67 ± 47.76	119.00 ± 36.22	112.44 ± 58.42	67.89 ± 35.67	278.91 ± 84.26
RCP8.5	2041-2060	115.50 ± 48.01	119.25 ± 36.05	113.81 ± 59.27	71.56 ± 35.37	280.07 ± 84.58
	2061-2080	125.66 ± 51.09	128.73 ± 37.95	124.21 ± 64.11	90.49 ± 34.73	310.61 ± 90.61

upscaling using the random forest method, SOC is estimated at 15.33 Pg within 0-3 m soil depth, 6.25 Pg within 3-6 m soil depth, and 28.85 Pg within 6-25 m soil depth (Wang et al., 2020). Although the soil layers (0-25 m) contain relatively small amounts of SOC on the TP, a larger percentage of the SOC is stored in the deeper soil layer (3-25 m) of the TP (70-80% of SOC stocks) than in deep layers in the circum-Arctic areas (only 39%). Mean topsoil (0-10 cm) organic carbon density (organic carbon amount per unit area) in the TP grassland is less than half of that in Arctic tundra (Wu et al., 2021), this discrepancy is largely due to the significant difference in soil carbon turnover times (547 years for the TP grassland relative to 1609 years for Arctic tundra), which is the average time elapsed between the sequestration of carbon and its release back to the atmosphere (Barrett, 2002). Large uncertainty exists in permafrost SOC, however, owing to the heterogeneous distribution of soil layers, ice content, regional variations, and limited SOC observations, particularly from the lack of deep borehole drilling (Mu et al., 2020). The estimated stock for the upper 2 m of soil ranges from 12.22 to 28 Pg (Ding et al., 2016; Cheng et al., 2019). Based on the boundary used in this study (Fig. 1; Liu et al., 2014a), the mean SOC content on the TP is estimated to be 29.8 g kg⁻¹ (Table 1), which is slightly less than onequarter of that found in the Arctic. The TP has less ground ice in total than that in the Arctic permafrost area, yet extensive permafrost degradation is more likely to occur in the TP due to its rugged topography, which increases carbon losses (Mu et al., 2020).

4. Past and future changes in permafrost characteristics

4.1. Ground temperature change

Permafrost temperatures have increased across the entire permafrost region in recent decades but exhibit strong spatial and temporal variability. The largest increases have occurred in the Canadian High Arctic, northern Alaska, and western Siberia, together with significant increases in the continuous permafrost of Russia and North America (Romanovsky et al., 2017). Across the entire Arctic, warm permafrost sites have displayed slower ground temperature increases than cold permafrost sites because the temperatures are already close to 0 °C. Sites in cold permafrost areas such as the Beaufort-Chukchi region, northern Alaska,

northwest Canada, northeastern Siberia, and Svalbard have experienced ground temperature increases ranging from 0.3° to $0.8~\mathrm{C}$ decade $^{-1}$ (Box et al., 2019; Richter-Menge et al., 2020), while at sites farther south within warm discontinuous permafrost, such as interior Alaska, the Mackenzie Valley, Scandinavia, and Russia, values of ground temperature over the last 30–40 years have increased at a lower rate, $<0.3~\mathrm{C}$ decade $^{-1}$ (Richter-Menge et al., 2020). At the DZAA, permafrost temperatures in the continuous permafrost zone increased by $0.39\pm0.15~\mathrm{C}$ from 2007 to 2016, and $0.20\pm0.10~\mathrm{C}$ in the discontinuous permafrost zone (Biskaborn et al., 2019). Based on 83 boreholes at different depths in the Arctic (Fig. 1; Biskaborn et al., 2019), the average MAGT increased at a rate of $0.23~\mathrm{C}$ decade $^{-1}$ in the last decade (Fig. 3a).

On the TP, nearly all monitoring sites displayed an increasing trend, at an average rate of $0.14\,^{\circ}\text{C}$ decade $^{-1}$ (Figs. 1 and 3a), which is less than in the Arctic. This is consistent with the slower air temperature warming on the TP compared with the Arctic. The MAGT increase has been characterized by strong temporal and spatial variability (Table 4). The temperature at the top of the permafrost for the sites along the QTH

Table 4 Observed mean annual ground temperature (MAGT) changes (${}^{\circ}$ C decade $^{-1}$) in the Arctic and the TP over the past years.

Region	Depth	MAGT change	Time period	Reference
Arctic	DZAA	0.39	2007–2016 for continuous permafrost	Biskaborn et al., 2019
		0.20	2007-2016 for	
			discontinuous permafrost	
	15.9	0.23	2007–2016	This study
	m			
TP	6 m	0.39	1996–2006	Wu and Zhang, 2008
		0.20	2006-2010	Wu et al., 2012a
	10 m	0.04-0.49	2005-2015	Streletskiy et al.,
	20 m	0.10 - 0.28	2005-2015	2017
	DZAA	0.12	2006-2010	Wu et al., 2012a
	20.2	0.14	2007-2016	This study
	m			
	40 m	0.12	2003–2015	Zhang et al., 2020

reached -0.9 °C in 2018, which was the highest since records began in 2004. The MAGT at a depth of 6 m increased at a rate of ${\sim}0.39~^{\circ}\text{C}$ decade⁻¹ over the period 1996–2006 (Wu and Zhang, 2008). Between 2006 and 2010, the increasing trend of 0.20 °C decade⁻¹ was less steep than the former period (Wu et al., 2012a). The permafrost temperatures at the depth of 10 m increased by 0.04-0.49 °C decade-1 and $0.10-0.28~^{\circ}\text{C}~\text{decade}^{-1}$ at 20 m from 2005 to 2015 (Streletskiy et al., 2017). Newly published permafrost data show a more rapid increase $(0.02-0.78 \, ^{\circ}\text{C decade}^{-1})$ for the depth of 10 m for the period 2004–2018 (Zhao et al., 2021). Influenced by surface features, subsurface water content, and soil thermal diffusivity, it generally takes one to two years for the changes in atmospheric temperature to propagate down to the DZAA. The MAGT at the DZAA, which is estimated to be 10–15 m on the TP (Zhou et al., 2000), rose at a rate of 0.12 $^{\circ}$ C decade $^{-1}$ between 2006 and 2010 (Wu et al., 2012a), which is slower than in the Arctic. At a depth of 40 m, the rate was 0.12 °C decade⁻¹ for the period 2003–2015 (Zhang et al., 2020). Similar to the Arctic, changes of cold permafrost (MAGT < -1.0 °C) on the TP are more distinct than those of warm permafrost (MAGT > -1.0 °C) (Wu et al., 2012a). More specifically, for deeper permafrost at a depth of 40 m, cold permafrost exhibited increases of 0.08–0.13 °C decade⁻¹, while the effect of warming on warm permafrost only reached 30 m depth (Zhang et al., 2020).

Overall, there are strong geographic heterogeneities of MAGT increases in both areas, wherein ground temperature increases are higher in cold permafrost than in warm permafrost. The Arctic has experienced

a more rapid increase in MAGT than the TP, because the Arctic contains more cold permafrost than the TP. This is especially true for the ice-rich permafrost areas, where latent heat effects related to melting ground ice play a key role in the permafrost temperatures approaching 0 °C, and mitigate the rate of ground temperature change (Romanovsky et al., 2010; Smith et al., 2010). Another possible cause is that the moist peat layers in the Arctic give rise to a higher contrast of thermal conductivity between freezing and thawing states compared to the TP with dry organic peat layers (McClymont et al., 2013) (Table 1). Strengthened vertical energy exchange between the ground surface and the underlying permafrost results in an area of preferential permafrost warming in the Arctic. In general, the permafrost warming that began three or four decades ago has been particularly rapid in cold-continuous permafrost.

The MAGT in the Arctic is projected to rise by 3.8 $^{\circ}$ C and 5.4 $^{\circ}$ C under the RCP 4.5 and RCP 8.5 scenarios, respectively, during the 2061–2080 period compared to the baseline period (2000–2014) (Fig. 4), while on the TP, the MAGT is predicted to increase by 1.9 $^{\circ}$ C and 2.9 $^{\circ}$ C under the RCP 4.5 and RCP 8.5 scenarios, respectively (Table 3), suggesting larger increases in MAGT in the Arctic than on the TP, especially under the high future emission scenario. This is in accordance with the projected MAAT changes that drive long-term permafrost temperatures.

4.2. Change in permafrost area

More than 40% of the permafrost areas (9.6 \times 10⁶ km²), equivalent

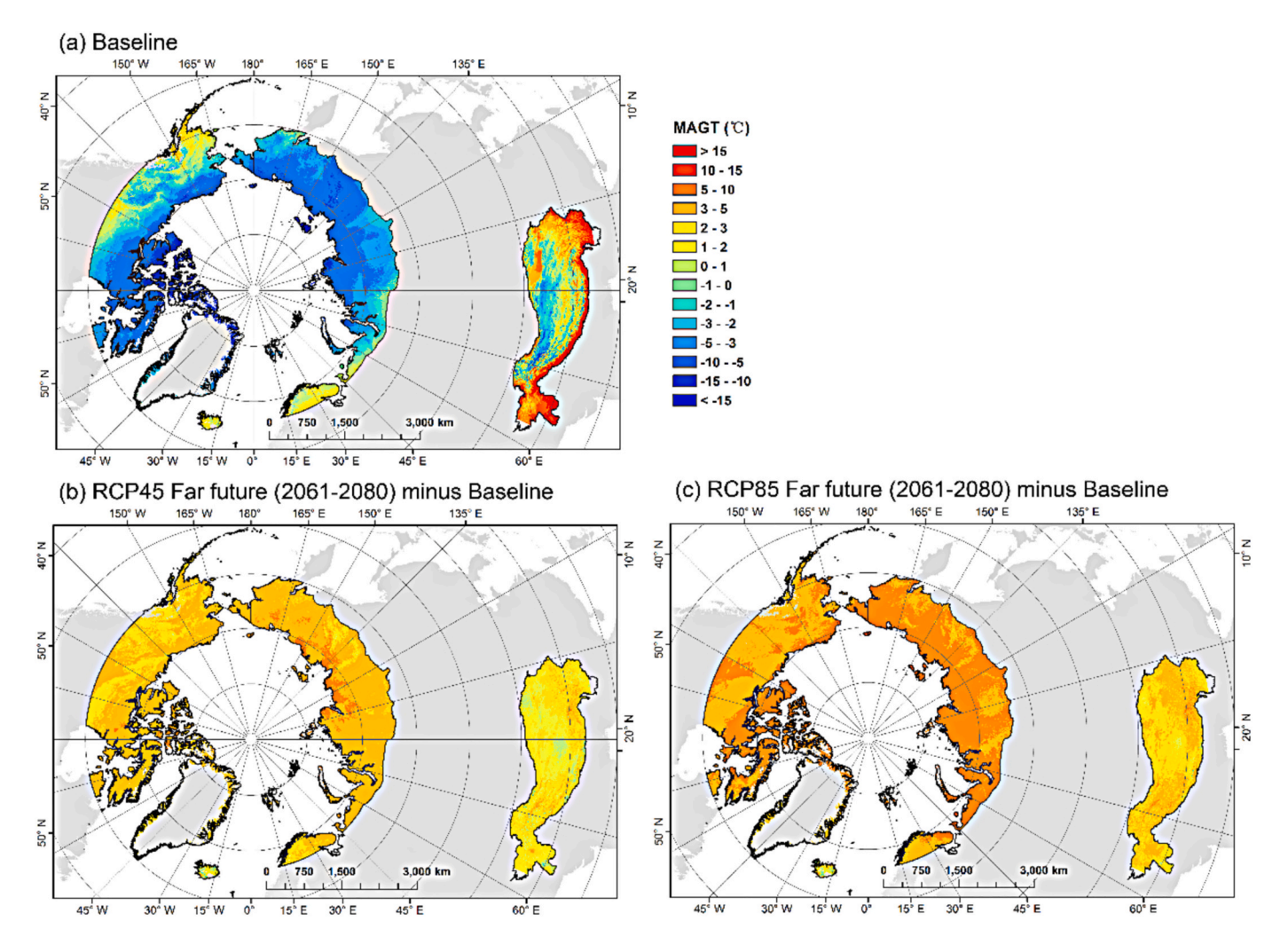


Fig. 4. Mean annual ground temperature (MAGT) in the Arctic and the TP for (a) the baseline (2000–2014) and MAGT changes for a few decades from now (2061–2080) under (b) RCP 4.5 and (c) RCP 8.5 relative to the baseline. The MAGT data for the Arctic is from Aalto et al. (2018). The MAGT data for the TP is from Ran et al. (2022), which employs the same method as that of Aalto et al. (2018) except that the driving data are the downscaled climate data from WorldClim.

to the Arctic permafrost area, are vulnerable to degradation, with a decreasing rate of $0.33 \times 10^6 \, \text{km}^2 \, \text{decade}^{-1}$ over the 1980–2009 period (Park et al., 2016). CMIP5 simulations have suggested that the sensitivity of permafrost primarily in the Arctic to global warming is approximately $4.0^{+1.0}_{-1.1} \times 10^6 \,\mathrm{km}^2 \,^{\circ}\mathrm{C}^{-1}$ (1 σ confidence) (Chadburn et al., 2017). The sensitivity in the CMIP6 multi-model ensemble lies between 3.1 and $3.8 \times 10^6 \text{ km}^2 \,^{\circ}\text{C}^{-1}$ (Burke et al., 2020), which falls at the lower end of the equilibrium sensitivity estimated by Chadburn et al. (2017). Over the past half-century, climate warming has caused permafrost degradation on the TP, but different degradation magnitudes have been reported. For example, the degradation rate simulated by Cheng et al. (2012) and Ran et al. (2018) using the MAAT model was $7.9-9.5 \times 10^4$ km² decade⁻¹ from the 1960s to the 2000s. The Community Land Model simulated the degradation rate over the TP to be $9.2 \times 10^4 \, \text{km}^2 \, \text{decade}^{-1}$ (Guo and Wang, 2013), which is within the above degradation range. The permafrost area on the TP decreased from $\sim 1.50 \times 10^6 \text{ km}^2 \text{ in } 1975$ to $\sim 1.26 \times 10^6 \text{ km}^2$ in 2006 (Jin et al., 2011) to the recent value of 1.06 \times 10⁶ km² over the period 2003–2012 (Zou et al., 2017), an overall decrease of approximately $0.44 \times 10^6 \text{ km}^2$ (or roughly a rate of $11.6 \times 10^6 \text{ km}^2$) $10^4 \text{ km}^2 \text{ decade}^{-1}$) from 1975 to 2012 (Yang et al., 2019).

In response to future climate warming, the permafrost area is projected to shrink in both regions. A process-based numerical model predicted that permafrost would prevail in the 21st century north of 70°N in the Arctic, and all areas north of 60°N would maintain permafrost at least at depth (Delisle, 2007). Compared with the 1960–1990 baseline, the permafrost area is predicted to decrease by $4.8^{+2.0}_{-2.2} \times 10^6$ km² under a 1.5 °C stabilization scenario by the end of the 21st century and $6.6^{+2.0}_{-2.2} \times 10^6$ km², or 40% of the current permafrost area, under a 2 °C stabilization scenario. This indicates that approximately 2×10^6 km² of permafrost (the equivalent of nearly twice the size of the TP permafrost) would be retained under a 1.5 °C stabilization scenario (Chadburn et al., 2017). The projected permafrost degradation is mainly located at the southern edge of the permafrost area for the Arctic as well as for the southern edge of the TP (Li and Cheng, 1999; Guo and Wang, 2016).

The future reduction in near-surface permafrost (permafrost in the topmost ground layers, < 10-15 m depth, Hjort et al., 2022) area exhibits different magnitudes in the two regions. In the Arctic, the nearsurface permafrost area is projected to gradually decline, from 22% (28%) in 2041-2060 to 29% (49%) in 2061-2080 under the RCP 4.5 (RCP 8.5) scenarios relative to the baseline (Table 3). This means that almost one-half of the near-surface permafrost would be lost by the end of the 21st century under the high emission scenario. In western Siberia, permafrost is projected by the CMIP6 models to disappear under SSP5-8.5 because of the MAAT 0 °C isocline moving toward the north (Alexandrov et al., 2021). On the TP, near-surface permafrost exhibits more rapid thaw than in the Arctic, especially under RCP 8.5: 58% in 2041-2060 and 84% in 2061-2080 (Table 3), indicating that nearsurface permafrost on the TP is more susceptible to rising air temperatures than the Arctic near-surface permafrost. The near-surface permafrost area on the TP is projected to decrease to 0.54×10^6 km² in 2099 under a future air temperature increase of 2.9 °C (warming magnitude under RCP 4.5) using an "altitude model" (Li and Cheng, 1999), which is close to the projection under RCP 4.5 (Table 3). It should be noted that these projections are essentially based on surface energy balance and heat conduction assumptions, which are likely to amplify permafrost thawing. Influenced by climate, vegetation, snow, and ground ice, permafrost thawing does not necessarily follow a linear trend. Zhao et al. (2020) argued that the permafrost table would deepen slowly, and some continuous permafrost would remain by 2050 under the RCP 8.5 scenario, with the lower boundary of the permafrost area (Xidatan) on the TP projected to still exist in 2100. This illustrates that there is great uncertainty in estimating permafrost degradation under future scenarios.

4.3. Active-layer thickness change

In the Arctic, the ALT has experienced an overall thickening since records began (Richter-Menge et al., 2020). According to the measurements at 142 CALM sites, the Arctic ALT increased at a rate of 0.15 cm yr⁻¹ from 1990 to 2019 (Figs. 1 and 3b), suggesting widespread, but modest permafrost degradation. The most obvious areas with increasing ALT are found in the Russian Europe North, eastern Siberia, and Chukotka, while the cold permafrost of Alaska and Canada has experienced small or no significant changes in ALT in recent decades (Peng et al., 2018). Numerical simulations indicate that the ALT in 24% of the permafrost in Alaska experienced a significant deepening trend from 2001 to 2015, and only a few areas (< 0.3%) displayed a significant decreasing trend; northern Alaska has a relatively small ALT trend (0.32 \pm 1.18 cm yr⁻¹), which is related to the colder climate and more stable permafrost conditions in this region; larger positive ALT trends (> 3 cm yr⁻¹) occurred across central and southern areas of Alaska, which feature a warmer climate and discontinuous permafrost conditions (Yi et al., 2018). Thus, the warm permafrost areas appear to be exhibiting greater magnitudes of ALT thickening compared to the cold permafrost areas. It is widely recognized that ALT will increase due to global warming, although other factors, such as snow cover changes, also provide significant contributions. Increases in winter snow depth and summer soil moisture are leading to soil temperature warming and ALT thickening in eastern Siberia (Park et al., 2016). The strong spring warming has caused a conspicuous advance of snowmelt and a longer snowless period, which have increased soil energy input and soil temperature, facilitating ALT deepening and permafrost degradation (Lawrence and Slater, 2010). Although the popular view that the warming climate has significantly increased ALT, some evidence indicates that the formation of thermokarst in ice-rich permafrost areas in Arctic Alaska may lead to a decrease in the ALT despite the warming because ground-ice dynamics and ecological feedbacks regulate the degradation and stabilization of ice wedges (Jorgenson et al., 2015; Kanevskiy et al., 2017). Vegetation (e.g., aquatic moss and herbaceous plant) colonization and accumulation of organic matter in the troughs that develop over degrading wedges result in decreased soil temperatures and thaw depths, as well as aggradation of new ground ice (Jorgenson et al., 2015).

For the TP, the magnitude of the ALT increase has also been higher in the warm permafrost areas than in the cold permafrost areas. The longterm and spatially averaged increase in ALT in the cold permafrost areas was \sim 5 cm yr⁻¹ from 1995 to 2007, which is significantly less than the 11.2 cm yr⁻¹ rate in the warm permafrost areas during the same period (Wu and Zhang, 2010). Regionally averaged ALT thickened at a rate of \sim 7.5 cm yr⁻¹ along the QTH from 1995 to 2007 (Wu and Zhang, 2010). Among the sites along the Qinghai-Tibetan Railway (QTR), the mean ALT between 2006 and 2010 increased at a rate of 6.3 cm yr⁻¹ et al., 2012a). These high rates are more likely related to local disturbances, given that a recent study indicated an average rate of 1.33 cm yr^{-1} along the QTH for the period 1981–2010 (Li et al., 2012b). ALT deepened further in 2018, reaching as much as 2.45 m, indicating that heat has penetrated deep into the permafrost, with the average increasing rate of the ALT from 1981 to 2018 reaching 1.95 cm yr⁻¹ (Fig. 3b).

By comparison, a greater increase in ALT has occurred on the TP (warm permafrost) than in the Arctic (cold permafrost). ALT changes are associated with relatively short-term fluctuations in climate and are particularly sensitive to summer air temperature change (Richter-Menge et al., 2020; Wu and Zhang, 2010). The air temperature increase in summer is higher in the Arctic than in the TP (Table 1). The thawing degree days (TDD, i.e., the cumulative number of degree-days above 0 °C per year) are manifesting a larger increasing trend on the TP than in the Arctic (Fig. 3c). This is consistent with the larger increase of ALT on the TP, suggesting that the increase in TDD enhances more soil energy input and contributes to the deepening of the ALT. The different

magnitudes of ALT increase can be explained by the TDD increase. For cold permafrost, a large quantity of energy entering the active layer and permafrost may be substantially expended for specific heat consumption from permafrost temperature increases and latent heat of fusion due to unfrozen water content. As for warm permafrost, most of the energy is used for melting the residual ground ice in permafrost, thus increasing ALT (Wu and Zhang, 2010). Therefore, the higher rate of ALT increase in warm permafrost compared to cold permafrost is primarily due to unfrozen water content changes with temperature.

The peat layer is probably another factor responsible for the small increase in the Arctic ALT. Over large swaths of the Arctic, the thick peat layer over continuous permafrost, as well as the thick peat layer with shrub and forest vegetation in discontinuous permafrost zones, is viewed as a strong buffer layer and substantially alleviates the impact of climate forcing on ALT (Smith et al., 2009). In contrast, on the TP, there is no peat layer and sometimes only bare ground, which enables climate forcing to exert a direct impact on ALT (Wu and Zhang, 2010). The regional response of the soil thermal regime to climate change is determined by differences in atmospheric warming and the current ground thermal regime.

The ALT is projected to undergo more drastic increases in the TP than in the Arctic in the future. The multi-model ensemble means of the CMIP5 models project that the largest increases (\sim 25–100 cm) will occur on the TP compared to the much smaller increases (<10 cm) in Alaska during the 2061–2080 period under the RCP 4.5 scenario relative to 2000–2014 (Fig. 5b). Under RCP 8.5, the ALT in the Arctic in the

2061–2080 period is projected to increase by \sim 25 cm on average, with the largest increase occurring in Greenland (41 cm). The ALTs in some permafrost areas of North America and Eurasia are projected to increase noticeably, and on the TP it is projected to increase by around 99 cm (Fig. 5c; Table 3). In general, the increase in ALT exhibits a decrease from south to north for both regions.

5. Permafrost degradation risk and potential impacts

Permafrost degradation caused by climate warming, including the loss of ground ice, has adversely impacted the stability of the ground surface, the integrity of hydrological systems (including water quality), ecosystems (including permafrost carbon emissions), and the socioeconomic systems in extensive areas of both the Arctic and the TP. These impacts have become increasingly observable and are projected to continue through the remainder of this century (IPCC, 2019). Below we review some of the main impacts and discuss regional differences.

5.1. Geohazard risk caused by permafrost degradation

The structure and functions of the Earth system are vulnerable to disturbances. Two identified core planetary boundaries including climate change and biosphere integrity might push the Earth system outside the safe operating space if crossed and that could also lead to deleterious or even disastrous consequences for humanity (Steffen et al., 2015). Surface instability, or potential geohazard, associated with

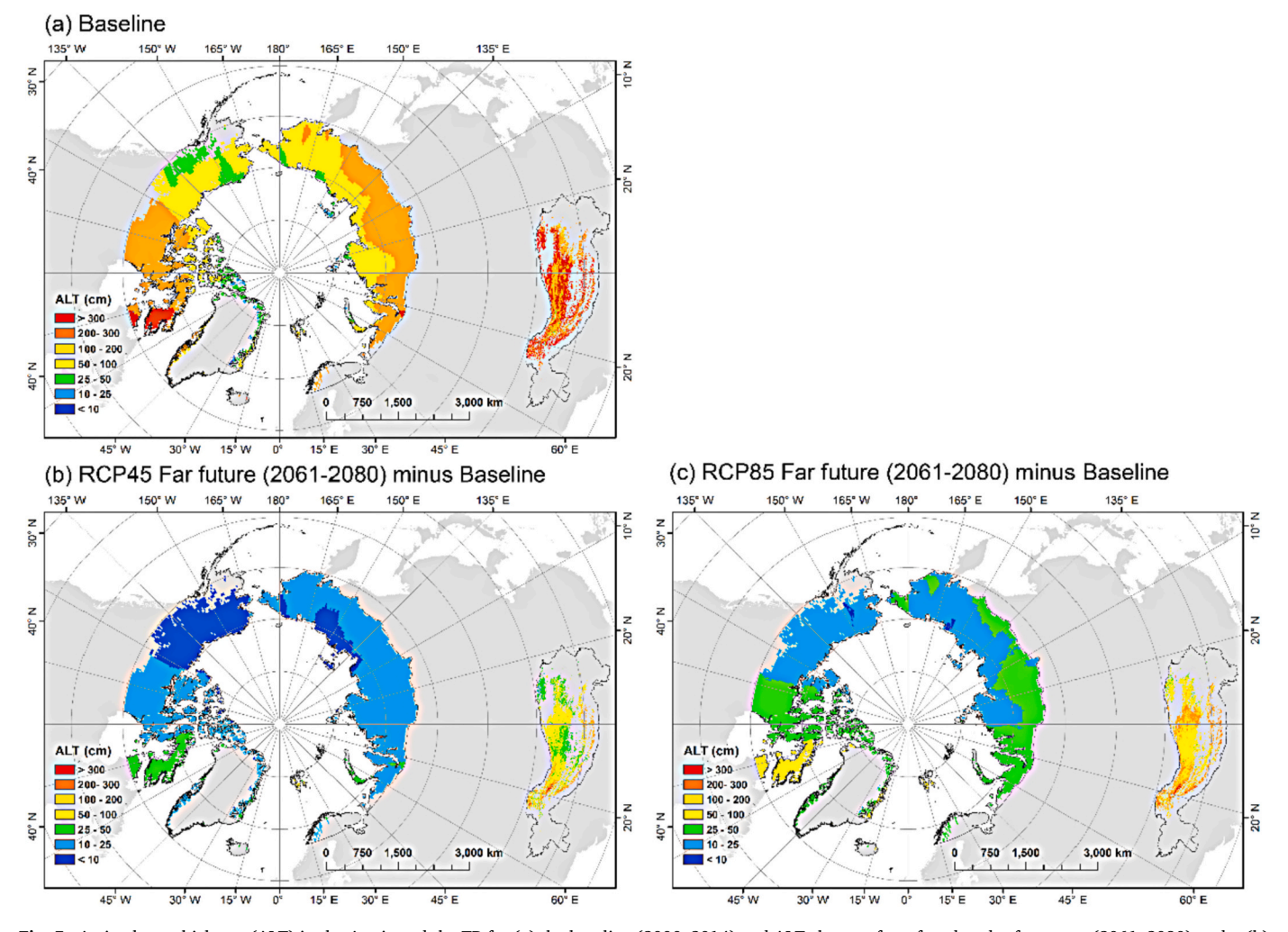


Fig. 5. Active-layer thickness (ALT) in the Arctic and the TP for (a) the baseline (2000–2014) and ALT changes for a few decades from now (2061–2080) under (b) RCP 4.5 and (c) RCP 8.5 relative to the baseline. The ALT data for the Arctic are obtained from Peng et al. (2018). The ALT data for the TP are from Ran et al. (2022).

permafrost degradation was mapped by Karjalainen et al. (2019a), taking into account ground ice content, soil grain size, and slope gradient. We used this analysis to compare geohazard risk between the Arctic and TP (Fig. 6). High-risk values are projected in the areas where the active layer is initially thin under RCP 4.5, such as western Siberia and Alaska; moderate risk values are distributed in extremely cold high-Arctic areas in which ice-rich permafrost is greatly disrupted by rapid thaw and erosion because high ground ice contents cause accelerated degradation by thermokarst and thermo-erosion processes (Kokelj and Jorgenson, 2013); and low hazard values predominate in northern Canada, which has large areas of rocky soils with little excess ground ice. Under RCP 4.5, the areas in the Arctic with high hazard risk for the 2041–2060 period is projected to increase 36.8% by 2061–2080, while under the high-emission scenario (RCP 8.5), the percentage reaches a level as high as 121.4%; in particular, a large portion of the Eurasian permafrost is projected to experience a high degree of hazard risk. On the TP, areas with low and moderate hazard risk are projected to decrease, and the area with high hazard risk could increase by 27.2% under RCP 4.5 and 23.4% under RCP 8.5 for the period 2061-2080 relative to 2041-2060. The reason for the smaller increase in high hazard risk for the RCP 8.5 scenario compared to the RCP 4.5 scenario is that a larger area of near-surface permafrost on the TP is projected to be lost under RCP 8.5, degrading into seasonally frozen ground or unfrozen ground and thereby reducing the instability of ground surface. As a result, the Arctic is more likely to experience more severe hazards due to permafrost degradation than the TP.

5.2. Impacts on the hydrological system

Permafrost greatly affects a wide range of hydrologic characteristics, including water storage, surface and subsurface flow patterns, discharge, water balance, and water quality. Permafrost retains large quantities of water resources over centuries or millennia in the form of ground ice, which are then released as the permafrost thaws. Permafrost thaw and degradation increasingly impact or restructure hydrological systems, including lake areas and the overall regional water cycle, with effects such as increased precipitation, evapotranspiration, and river and groundwater discharge (amount and timing of runoff) (Fig. 7), especially across those regions with well-developed permafrost (Walvoord and Kurylyk, 2016; Ding et al., 2019; IPCC, 2019; Su et al., 2019). Permafrost degradation can also induce releases of heavy metals and toxic contaminants, such as mercury and arsenic, further lowering the water quality for freshwater biota, drinking water, and agriculture irrigation, which is potentially harmful to human health (Colombo et al., 2018; Miner et al., 2021; Vonk et al., 2015). The observed hydrological effects have indicated a comparably homogenous pattern. The increments of streamflow are strengthened where extensive permafrost underlies much of the landscape. It shows a high annual maximum/ minimum discharge ratio, while the discharge ratio changes slightly in low permafrost coverage basins (Gruber et al., 2017; Song et al., 2019).

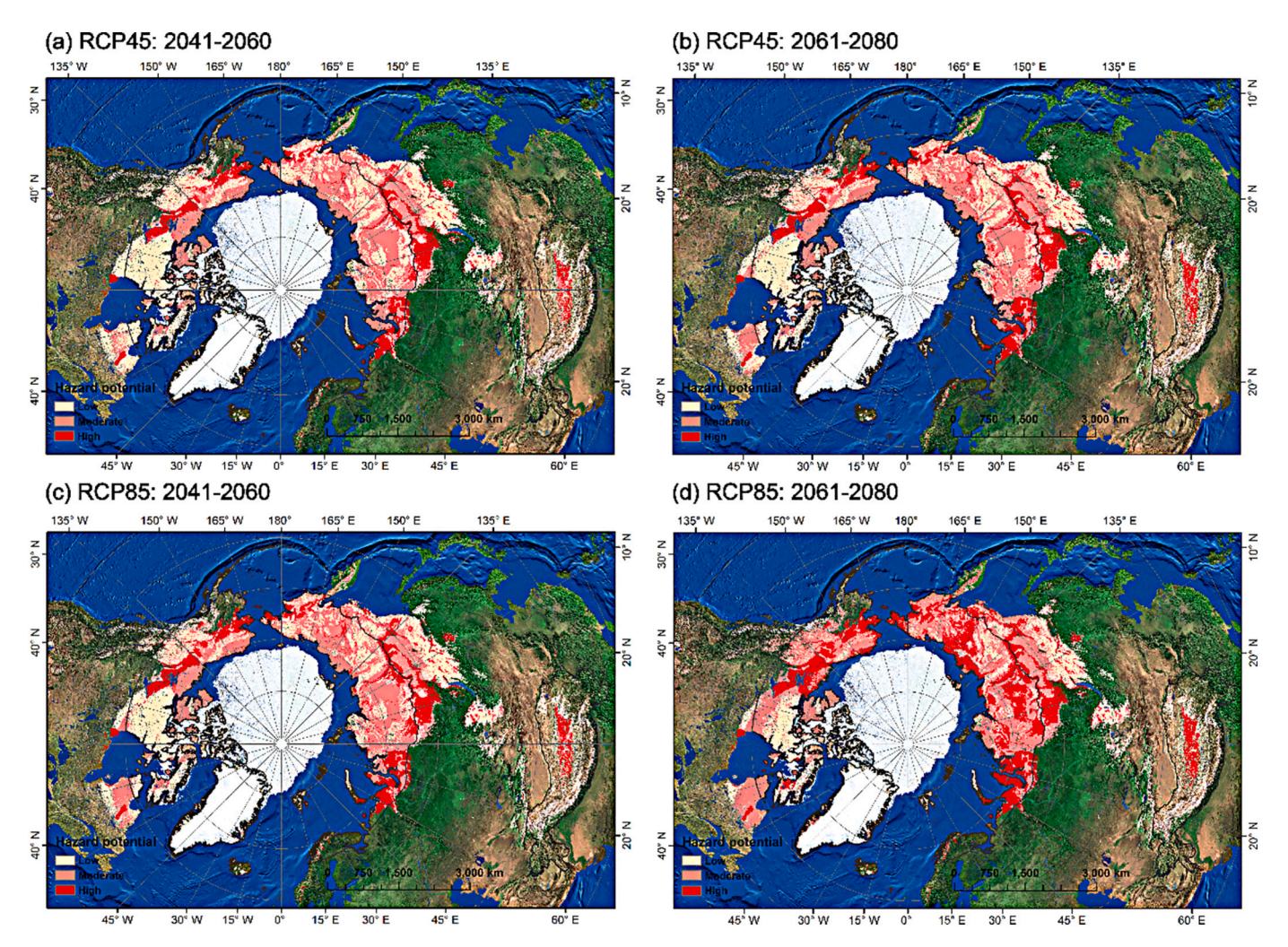


Fig. 6. Projected geohazard indices showing permafrost degradation associated risks to infrastructure under RCP 4.5 (top row) and RCP 8.5 (bottom row) scenarios for the mid-future (2041–2060) (left column) and far-future (2061–2080) (right column). The index reflects a consensus of geohazard indices and includes three classes delimiting areas of low, moderate, and high hazard potential. Data source: Karjalainen et al. (2019a).

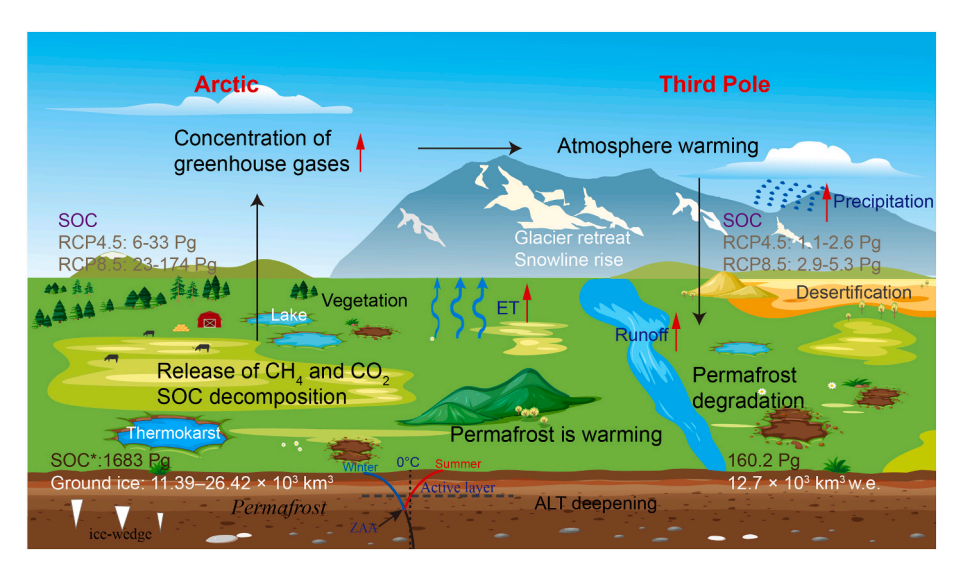


Fig. 7. Influence of permafrost degradation on hydrology and ecosystems. SOC* indicates the estimated current soil organic carbon. The values of ground ice and SOC are sourced from previous studies, which are correspondingly cited in the main text.

Many large river basins are distributed across the pan-Arctic region, such as the Ob, Yenisei, Lena, and North East Siberia in Eurasia, and the Yukon, Mackenzie, Nelson, and North and South Hudson Bays in North America. Rennermalm et al. (2010) showed that an increasing coldseason low-flow is apparent over most of the pan-Arctic river discharge systems during the 20th century, with the decreasing flow in eastern North America and unchanged flow in mainly small basins in eastern Eurasia in the late-20th century. The surface water area has decreased in the discontinuous permafrost areas of western Canada, central and southern Siberia, and interior Alaska (Lantz and Turner, 2015). Warming-induced changes in permafrost have led to a remarkable shift toward an increase in the winter and early spring streamflow of Siberian rivers (Melnikov et al., 2019; Song et al., 2019). Moreover, as a result of permafrost thawing, Siberian groundwater discharge to rivers has been enhanced with every 1 °C increase in air temperature likely causing a 6.1-10.5% increase in groundwater discharge, depending on permafrost condition (Wang et al., 2021b). Meanwhile, thermokarst lakes in the continuous permafrost areas of northern Siberia and Alaska have expanded (Polishchuk et al., 2015), and the area of small lakes in the Arctic is projected to increase more than 50% by 2100 under RCP 8.5 (IPCC, 2019). The drainage of lakes in discontinuous to continuous permafrost areas in the Arctic, such as in western Siberia and Alaska, has increased because of permafrost degradation, which may signify that changes in thermokarst lakes are associated with the transition between different hydrological regimes when permafrost becomes increasingly discontinuous (Nitze et al., 2018). In addition, more developed thermokarst lakes are conducive to accelerating permafrost thaw through rising ground temperature above freezing.

The TP is the source of many large Asian rivers, providing an annual river runoff of 656 ± 23 billion m³ in 2018, with the largest contribution to the Ganges River (Wang et al., 2021a), and has developed numerous alpine lakes, features whose hydrological regimes are closely regulated by permafrost. River runoff has increased on most of the TP due to an increase in unfrozen water content caused by rising ground temperature (e.g., Qiu, 2012; Zhang et al., 2017; Li et al., 2019). Ground ice melt contributed 12% of the water supply to the increased lake volume in the TP's endorheic basin from 2011 to 2015 (Zhang et al., 2017). In the Qilian Mountains, the meltwater from permafrost thaw is estimated to have been 1.18 km³ a $^{-1}$ over the past 10 years, accounting for 10% of annual runoff at the mountain outlets (Li et al., 2019). However, a few studies suggested that permafrost thawing may decrease winter river runoff in certain areas of the TP (Wang et al., 2009; Qiu, 2012; Gao et al., 2016). For example, winter river runoff has decreased on the northern

TP, mainly as a result of active layer thickening (Gao et al., 2016), which likely absorbs more water that otherwise would have flowed into the river. The hydrology reacts to warming permafrost differently between the TP and the Arctic because the runoff from permafrost into rivers is jointly dictated by permafrost temperatures, permafrost type, permafrost thaw depth, and vegetation cover (Wang et al., 2009; Qiu, 2012). Compared to the Arctic permafrost, for instance, most permafrost in the northern TP belongs to discontinuous permafrost, which allows more soil liquid water infiltrate to deeper underground, thereby decreasing surface discharge. The decrease of vegetation cover can boost active soil thawing, and therefore reduce surface runoff during freeze-thaw processes (Wang et al., 2009). The number and coverage of thermokarst lakes in the TP have increased by approximately 534 and 410 ha between 1969 and 2010 in the Beilu River Basin, respectively (Luo et al., 2015). By contrast, in the Arctic river basins, compared to annual discharge changes, the baseflow changes are more closely associated with the permafrost extent of a watershed, while for the TP basins, the permafrost extent plays a more predominant role in the annual discharge changes (Song et al., 2019). Thawing permafrost can also contribute to streamflow and sea-level rise. When permafrost thaws, some meltwater flows to rivers and oceans. If all the permafrost in the NH thawed, the water released from ground ice would increase the global sea level by 2.7 to 8.8 cm (Zhang et al., 2000). This is especially pronounced in the Arctic with its large volume of ground ice. For the TP, meltwater generally enters rivers and lakes (Zhang et al., 2017; Zhao et al., 2019), thereby having large consequences for regional water resources and security. Because the response of permafrost to climate warming is a slow and long-term process, the influence of permafrost degradation on the hydrological process is expected to be a gradual process.

5.3. Impacts on ecosystems

Ecosystems in permafrost regions are diverse because of strong spatial heterogeneities in environmental conditions and disturbance regimes (Walker et al., 2005; Jorgenson and Grosse, 2016). Permafrost plays a crucial role in the formation and development of vegetation and ecosystems, as well as organic carbon decomposition, based on the processes of water conservation and water-thermal regulation (Yang et al., 2010; Koven et al., 2011; Natali et al., 2019; Su et al., 2019).

In recent decades, permafrost degradation has markedly altered species composition and abundance, as well as caused shifts in habitat and biome of ecosystems through changes in soil temperature and moisture, as well as permafrost permeability (Jorgenson et al., 2013; Schuur and Mack, 2018). For instance, Myers-Smith et al. (2011) complied numerous observations of increases in shrub species in tundra ecosystems across the circumpolar Arctic. In the tundra of the northern Arctic, permafrost thaw has significantly impacted wetlands. Some wetlands have dried up while other new wetlands have appeared (Su et al., 2019). Such changes can substantially alter animal habitats (Marcot et al., 2015). Thermokarst can influence 10–30% of the Arctic lowland landscapes and greatly alter tundra ecosystems (Jorgenson et al., 2006). On the TP, permafrost thaw has already caused ecosystem deterioration, especially in the eastern and western portions, in which large areas of alpine meadow and alpine wetland ecosystems have been degraded, and the area affected by desertification has increased significantly (Yang et al., 2010). As ecosystems transition from permafrost to non-permafrost systems, aboveground net primary production will drop over most of the TP (Yang et al., 2018). Conversely, in some alpine regions, plant productivity has increased due to increased soil water from underlying permafrost thaw (Yang et al., 2018). Overall, permafrost degradation has significantly altered the structure and functions of the ecosystems in both regions, but the impacts show a certain latitudinal dependency in the Arctic and both latitudinal and elevational dependency in the TP.

Climate warming and other human activities could trigger biosphere tipping points across a variety of ecosystems and scales, which can cause a quick and irreversible (on human time scales) release of carbon back to the atmosphere, thereby magnifying climate change (Schaefer et al., 2014; Lenton et al., 2019). Several studies have indicated that ecological systems in the Arctic may transform from a carbon sink to a CO2 source by the end of the 21st century (Koven et al., 2011; Natali et al., 2019). Potential carbon release in the circum-Arctic permafrost zone ranges from 6 to 33 Pg C and from 23 to 174 Pg C by 2100 under the RCP 4.5 and RCP 8.5 scenarios, respectively (Anthony et al., 2018). SOC over the TP is projected to decrease as well. A recent estimate indicated 1.07-2.60 Pg C and 2.87-5.30 Pg C emissions by 2100 for RCP 4.5 and RCP 8.5, respectively (Wang et al., 2020), accounting for 3-43% and 2-23% of the SOC emissions in the circum-Arctic region estimated by Anthony et al. (2018). Moreover, permafrost carbon thawing from deep layers (> 3 m), where a large proportion of permafrost carbon is sequestered, could comprise at least 30% of the total permafrost carbon loss on the TP. A currently observed alpine steppe ecosystem has turned from a carbon sink into a source (Yun et al., 2022). As the frozen organic material thaws and decays, the emissions of methane and CO₂ add to the concentration of greenhouse gases in the atmosphere, further enhancing the warming (Fig. 7), especially in the susceptible polar regions. The permafrost carbon feedback could increase the global temperature by $0.29\pm0.21~^{\circ}\text{C}$ (7.8 \pm 5.7%) by 2100 under RCP 8.5 (Schaefer et al., 2014). Coastal erosion in the Arctic could amplify climate warming in that rapid sea-level rise in the past suggests that shelf erosion was the dominant process for the release of greenhouse gases from permafrost in the Arctic shelf area (Winterfeld et al., 2018). In contrast, coastal erosion is not a factor in the TP.

The real world is facing a new threat of long-dormant microbes (such as bacteria and viruses) trapped in permafrost that could now be revived upon thawing in a warming climate (Revich and Podolnaya, 2011; Walsh et al., 2018; IPCC, 2019). Pathogenic viruses and microbes preserved in permafrost regions have been found to remain alive for lengthy periods (Tumpey et al., 2005; Legendre et al., 2014). As a consequence of permafrost thawing, the exposure to contaminated sources such as buried carcasses, cemeteries, and fossils could lead to the release of present and future mysterious viruses (Zerefos et al., 2020). There are some possibilities that viruses resulting from melting glaciers or thawing permafrost in the Arctic can be transferred by the wind and migratory birds, as well as spread along water systems to lower latitudes (IPCC, 2019; Zerefos et al., 2020). These studies highlight that the thawing of older permafrost layers expected in the upcoming decades, especially in the post-COVID-19 period may herald novel and unknown epidemics,

posing new horrifying threats to animals and human beings. In high-latitude and high-altitude areas of Asia, such as those surrounding the TP, soil nematode density reaches a high level (van den Hoogen et al., 2019). Although no similar studies have been conducted for the TP, it is most likely that similar concerns can be expressed for the TP, which calls for future studies on this aspect. Meanwhile, prompt action to slow permafrost thaw can be a major strategy for mitigating threats from biological hazards.

5.4. Socioeconomic effects

Permafrost carbon feedback, one of eight climate tipping points identified by Dietz et al. (2021), contributes to an 8.4% increase in the social cost of carbon, only slightly lower than the largest contribution from the dissociation of ocean methane hydrates (13.1%) (Dietz et al., 2021). Owing to permafrost thaw, the melting of ground ice, and increased water flow on frozen slopes, the stability of mountainsides is decreasing, which can trigger landslides and cascading events. Simultaneously, retrogressive thaw erosion has become much more common. As a result, landforms such as thawed slumps and thermokarst lakes have expanded (Rowland et al., 2010; Jorgenson and Grosse, 2016; IPCC, 2019). Such processes can produce detrimental impacts on engineered structures, such as towns, buildings, roads, pipelines, oil and gas infrastructure, and dams, and further affect the utilization of natural resources and the sustainable development of the socioeconomy (Nelson et al., 2001; Melvin et al., 2017; Hjort et al., 2018). The large impacts on infrastructure from degrading permafrost are related to the widespread decrease in the bearing capacity of the frozen ground because of increasing permafrost temperatures and the differential subsidence of the ground surface caused by the thawing of ice-rich permafrost (Streletskiy et al., 2019).

The socioeconomic effects of rapidly degrading permafrost in the Arctic have become increasingly worrisome in recent years. Hjort et al. (2018) suggested that degrading permafrost will put much of the Arctic's infrastructure at risk by 2050. Approximately four million people and 70% of the current Arctic infrastructure are located in the permafrost region with high hazard risk, and one-third of the pan-Arctic infrastructure is in the area with thawing-induced ground instability. Coastal erosion and thawing permafrost have threatened numerous coastal and riverine communities, especially in Alaska (Larsen et al., 2008; Hong et al., 2014). The socioeconomic impacts of permafrost thaw on public infrastructure are considerable. If no adaptation measures are undertaken, it is estimated that the total expenses from near-surface permafrost thaw-related damage to infrastructure in Alaska from 2015 to 2099 could amount to US \$1.6 billion and US \$2.1 billion (2015 dollars, 3% discount) under the RCP 4.5 and RCP 8.5 scenarios, respectively (Melvin et al., 2017). Permafrost thaw also affects nonrenewable resource (e.g., hydrocarbon) extraction in the Arctic (IPCC, 2019). On the TP, with a population of about 5.6 million based on the Landscan Global 2019 dataset (Rose et al., 2020), many studies have demonstrated that permafrost thaw negatively impacts engineered structures, such as the QTH, the QTR, and buildings (e.g., Yang et al., 2010; Gruber et al., 2017; Hjort et al., 2018), while the socioeconomic consequences are still largely unknown. In comparison with the TP, more human activities occur in the Arctic permafrost regions and engineered structures are associated with permafrost dynamics to a greater extent. As a result, socio-economic activities are bound to be strongly affected by permafrost changes. With the aid of upgraded permafrost projections, detailed hazard maps, and identified infrastructure data, quantitatively estimating the economic impacts of permafrost degradation on infrastructure in both areas would be achievable (e.g., following Melvin et al., 2017).

6. Possible connections between the Arctic and TP

6.1. Interactions between land/ocean and atmosphere in the two regions

To better understand the possible linkages between the Arctic and the TP, a diagram of land-ocean–atmosphere interactions in each region is presented in Fig. 8. In the Arctic, the surface-albedo positive feedback is a major mechanism responsible for the Arctic amplification (Cohen et al., 2018), although the exact role of the albedo feedback is still under debate. Another positive feedback effect exists between climate warming and vegetation growth (Chapin et al., 2005; Pearson et al., 2013; Jeong et al., 2014). Climate warming enhances vegetation growth, which decreases surface albedo, and this, in turn, warms the climate via the radiation balance. In general, permafrost degradation causes vegetation growth due to snow melting and soil moistening, thus increasing air temperatures (Jeong et al., 2012, 2014). Enhanced vegetation productivity, particularly for shrub expansion, reduces surface reflection

and increases evapotranspiration (Loranty and Goetz, 2012). Earth system model simulations suggest a hypothetical 20% increase in shrub cover in the Arctic can provide a positive feedback to ongoing climate warming (Bonfils et al., 2012).

While albedo differences related to vegetation height and types have been noted in the Arctic ecosystems (e.g., Loranty and Goetz, 2012; Helbig et al., 2016). In the sporadic permafrost zone of North America, permafrost thaw induces a shift from forests to wetlands and that leads to an increase in albedo, which retards warming trends and alters regional precipitation regimes through drastically changing the Bowen ratio (sensible heat flux divided by latent heat flux) (Helbig et al., 2016). Similar to the southern Taiga Plains, thawing permafrost collapses birch forests but with a concurrent expansion of wetland area in the Tanana Flats in central Alaska (Jorgenson et al., 2001; Lara et al., 2016). Through all of these processes, permafrost thaw-caused land cover changes exert an influence on the key processes in land-atmosphere interactions and subsequent surface climate. Climate feedbacks due to

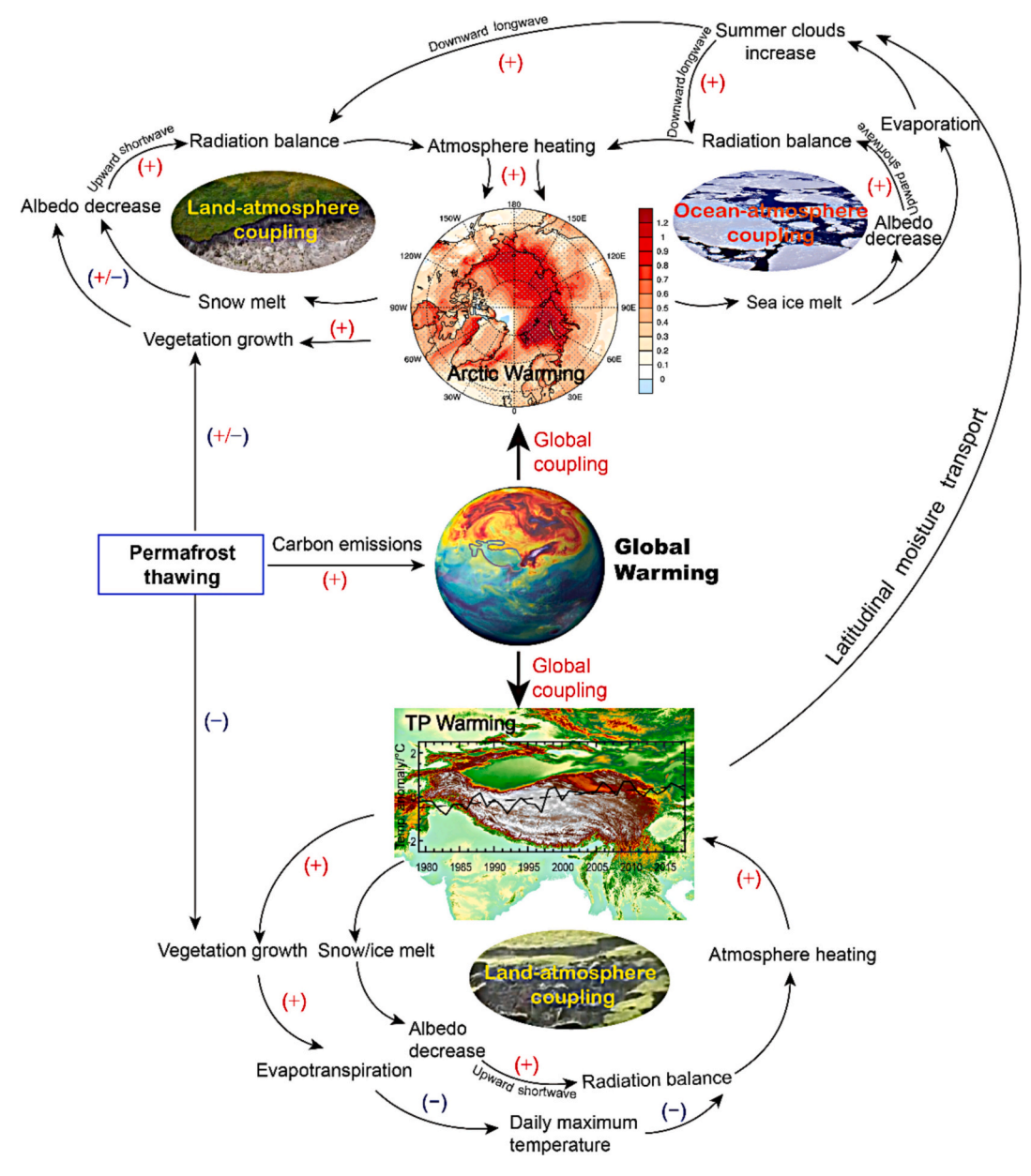


Fig. 8. Diagram of feedback loops that couple climatic processes and possible connection between the two polar regions (modified after Chapin et al., 2005). The temperature trends (1979–2018) were calculated using the ERA5 reanalysis (Hersbach et al., 2020) for the Arctic (including the Arctic Ocean) and the CRU dataset (Mitchell and Jones, 2005) for the TP.

ocean—atmosphere coupling, such as the sea-ice albedo feedback and the turbulent heat fluxes from ice-free areas of the Arctic Ocean, are also important factors for AA (Cohen et al., 2018). The continuous rapid sea-ice loss in the Arctic enhances heat accumulation and has an impact on snow cover, increasing the vulnerability of permafrost degradation under increased warming, there is therefore an indirect link between abrupt sea ice loss and permafrost health (Lawrence et al., 2008).

The frequent freeze-thaw processes in the permafrost region modulate the soil heat balance and strengthen heat exchange in landatmosphere system on the TP (Li et al., 2012b; Yang et al., 2019). Permafrost degradation has a large impact on energy-water exchange processes between land and the atmosphere, and these physical processes further influence the Asian monsoon system and associated regional climate (Yang et al., 2010; Yang and Wang, 2019). In contrast to the Arctic, a negative feedback seems to exist between climate warming and vegetation growth on the TP (Shen et al., 2015). Climate warming increases vegetation growth through improved growing conditions which lead to decreased albedo (Pang et al., 2022); meanwhile, evapotranspiration is enhanced by the increased vegetation growth due to the strong solar radiation over the plateau's surface. This significantly reduces temperatures through evaporative cooling and offsets the warming caused by the decreased albedo, thus reducing climate warming (Shen et al., 2015). Permafrost degradation on the TP, however, limits vegetation growth due to the ALT deepening and soil drying (Jin et al., 2021), which eventually enhances climate warming. Various causes, such as surface (snow)-albedo feedback and water vapor change, have been proposed to account for prominent elevation-dependent warming (Pepin et al., 2015; You et al., 2020).

For both regions, clear-sky downward longwave radiation affected by atmospheric water vapor has recently been diagnosed to be the dominant factor regulating surface temperature change (Gao et al., 2019). Climate warming exerts a tremendous influence on permafrost and affects surface energy partitioning, which can trigger a set of interlinked feedback processes that further alter the local and global climate (Chapin et al., 2005; Teufel and Sushama, 2019). The seasonally frozen status of the NH permafrost has experienced advancing and lengthening non-frozen season trends, which have made significant contributions to annual evapotranspiration (Zhang et al., 2011). In addition to permafrost carbon feedback, permafrost degradation has changed soil water contents i.e., drier ground surface, and the energy partitioning (Lund et al., 2014), which could restrain cloud development and enhance downward shortwave radiation and land surface temperatures (Ford and Frauenfeld, 2016).

6.2. Connection between the two regions

Close examination of the connections between the Arctic and TP contributes to an enhanced understanding of climate-change mechanisms and the interactions between climate and permafrost. There is evidence that a possible link between the two polar regions comes from the influence of the Arctic on the TP, because the enhanced AA effect and rapid climate warming of the Arctic and associated sea-ice reduction significantly impact the global climate system (Huang et al., 2017; Gao et al., 2020). AA in turn is likely to lead to enhanced warming over the TP because the Arctic amplifies the climate system's response to anthropogenic forcing and the TP is one of the most sensitive areas in the global climate system. The rapid warming of the Arctic climate has likely exerted significant influences on the TP's weather and climate systems through the weakening of the poleward temperature gradient (Coumou et al., 2015; Wang et al., 2018c), Rossby waves (Gao et al., 2020), and teleconnections such as the polar vortex, Arctic Oscillation (Jeong et al., 2012), North Atlantic Oscillation (NAO) (Linderholm et al., 2011), and Atlantic Multidecadal Variability (Shi et al., 2019).

The effect of the NAO on TP precipitation has attracted widespread attention in recent years (Liu et al., 2015; Wang et al., 2018a). A previous study has indicated that the upstream NAO has a significant

impact on the dipole oscillation of the TP summer precipitation through modulation of the atmospheric circulation over and around the TP (Liu et al., 2015). It is worth noting that an influx of freshwater is driven by Arctic warming and Greenland Ice Sheet melting into the North Atlantic. This could have led to a weakening of the Atlantic Meridional Overturning Circulation by about 15% since the mid-twentieth century (Caesar et al., 2018), which could also interrupt the East Asian monsoon (Lenton et al., 2019). More recent research has suggested that the springtime land-surface temperature anomaly on the TP is linked with the wintertime wave activities in the Arctic region. The wave trains from the Arctic can propagate and reach the TP, which favors TP snowfall, thereby influencing the springtime land-surface temperature (Zhang et al., 2019). This pattern is still being explored because of a lack of reliable datasets (observations and model simulations) and warrants further investigation given that the Arctic may impose much broader and longer-lasting impacts on the Asian climate.

Many studies have argued about the influences of Arctic warming on weather and climate in the mid-latitudes. Observational analyses have suggested that warmer winter temperatures in the Arctic have contributed to cooling over the mid-latitudes from 2000 to 2013 (Cohen et al., 2020), but more recent observations challenge this conclusion (Blackport and Screen, 2020). Findings from modeling studies are divergent (Cohen et al., 2020), with some studies finding a significant connection between AA and mid-latitude cooling (Honda et al., 2009; Mori et al., 2014), while others find little to no systematic influences of AA on midlatitude weather (Dai and Song, 2020; McCusker et al., 2016). The issue of Arctic and mid-latitude connections is complicated by the short observational time series, small signal-to-noise ratio, and the large influence of internal variability (Overland, 2016), and may have been underestimated by models due to model deficiencies (Mori et al., 2019). Furthermore, the AA response can be highly non-linear (Chen et al., 2016b; Overland, 2016), and may depend on the background state (Overland et al., 2021) and the location of sea ice loss (Chen et al., 2016a; Screen, 2017). Therefore, appreciable knowledge gaps exist regarding the effects of Arctic sea ice and AA mechanisms on midlatitudes, as well as discrepancies in both observations and model simulations (McCusker et al., 2016; Cohen et al., 2020).

Research on feedbacks from the TP to the Arctic is relatively scarce. Nevertheless, some studies have attempted to explore the connection caused by TP snow cover forcing. For instance, seasonal snow cover on the TP has been revealed to modulate the El Niño-Southern Oscillation (Wu et al., 2012b) and to affect the East Asian summer monsoon as well as the plum rain (i.e., East Asian rainy season) (Liu et al., 2014b; Zhu et al., 2015). More broadly, autumn TP snow cover has been suggested as an explanation for the downstream North America extreme cold event of 2009/2010 (Lin and Wu, 2011). The strong TP surface cooling caused by snow cover anomalies over the TP can excite a Pacific-North Americalike atmospheric response (Liu et al., 2017). Further research has indicated that abnormal autumn snow cover over the eastern TP can induce a hemisphere-scale wave train pattern, which crosses the North Pacific Ocean and reaches the North American region where it affects winter temperatures over western and eastern North America (Qian et al., 2019).

Another possible connection between the two regions is latitudinal moisture flux transport from the TP to the Arctic. Seasonal persistence of soil moisture anomalies associated with permafrost on the TP significantly influences precipitation in downstream areas (Yang and Wang, 2019). Soil water-heat state anomalies caused by permafrost may enhance TP thermal forcing to the subtropical westerlies and affect stationary Rossby wave train propagation in the mid-latitudes, thereby inducing downstream fluctuation of weather and climate (Fu et al., 2020). The humidification of the Arctic, characterized by increases in soil moisture, river discharge, and precipitation, is partly due to enhanced poleward atmospheric moisture transport from the mid-latitudes (Zhang et al., 2013).

7. Future outlooks

Permafrost research has made enormous progress over the last four decades, yet several issues remain unsolved and require more attention in future research. To better understand the climate changes that have occurred over recent decades and to appropriately predict whether future changes will approach a global cascade of tipping points (Lenton et al., 2019), large knowledge gaps remain regarding permafrost characteristics, ecological feedbacks, and extreme events. These can be aided by improvements in remote sensing, numerical models, integration of field observations with the rapid advancement in the big data era (Jorgenson and Grosse, 2016; Yang et al., 2019; Guo et al., 2020; Jiang et al., 2020; Li et al., 2020).

Permafrost mapping still involves substantial uncertainties due to a lack of explicit and standardized mapping criteria, appropriate unified classification systems, and high-quality field data, despite the growing availability of observational data (Brown et al., 2002; Ran et al., 2012). Currently, the most widely used permafrost map presents the past permafrost distribution, but cannot reflect the situation after 2000, especially given the rapid climate warming. Ground ice is estimated based on the outdated permafrost map and limited field investigations; this parameter, together with permafrost area and the thickness of sediment with ground ice, are in a generalized fashion. To obtain a spatially explicit estimation of organic carbon stocks in the two regions, special efforts should be made to investigate deep carbon dynamics across permafrost regions (Ding et al., 2016; Mu et al., 2020). The high degree of spatial heterogeneity illustrates the significance of highresolution mapping of global permafrost for infrastructure planning and understanding the impacts of permafrost thaw on hydrology and ecosystems. A recompiled permafrost map is recommended based upon thorough on-site observational data (e.g., borehole samples) with longterm and extensive spatial coverage, high-resolution satellite data, and climate model simulations, and should furthermore incorporate ever more prevalent machine learning and data assimilation methods.

Ground temperatures that are simulated in many models of permafrost dynamics rely heavily on linear relationships between air temperature and permafrost area, and also on the assumption of an unchanging present-day relationship between MAGT and permafrost (Chadburn et al., 2017), yet the effects of the thermal inertia of deep soil layers or geothermal heat flux have been routinely ignored (Wu et al., 2010). In the climate-driven permafrost zone, a close linear relationship between air temperature and ground temperature can be obtained, but it is not the case in other areas with ecosystem-driven permafrost (Karjalainen et al., 2019a). Other environmental factors can also exert crucial influences on permafrost. The highly variable buffer layers, such as vegetation, snow cover, and soil organic layers, together with soil properties and precipitation, complicate geophysical trends (Biskaborn et al., 2019; Karjalainen et al., 2019b; Zhang et al., 2021). Remote sensing-based data and techniques, combined with process-based modeling (including dynamic vegetations), have the potential to include multiple factors and their interactions, making modeling more realistic and thereby proving additional insights into the permafrost changes (Wang et al., 2016; Yang et al., 2019; Jiang et al., 2020).

There are large discrepancies in the simulations of near-surface permafrost area, ALT by CMIP5/6 GCMs, and the magnitude and timing of carbon emission as well as their impacts on climate change. These have been ascribed to the differences in simulated surface climate, such as AA intensity (Cohen et al., 2018), as well as the diverse capabilities of land surface models to describe thermal physics and snow (Lawrence et al., 2012; Slater and Lawrence, 2013; Zhu et al., 2019). In addition, different permafrost types exert diverse influences on climate due to differences in soil moisture, soil organic content, and vegetation (Jiang et al., 2020), although the involved interaction processes have been poorly understood. Projections of future permafrost dynamics rarely consider the impact of potential changes in SOC on soil temperature and permafrost area (Zhu et al., 2019). Also lacking is a better

understanding of the effects of latent heat associated with high ground ice contents that vary with depth and progressive thawing that leads to talik formation beneath the active layer, such as the boreal zone where permafrost is strongly affected by ecosystem dynamics. The uncertainties that result in the large divergence in the simulation of permafrost change highlight the need for model improvements, particularly for the ability to capture a sequence of couplings and feedbacks in the Earth system, both locally and remotely. The differences in permafrost dynamics and their drivers over both regions are necessary to be considered in Earth system models.

There have already been reports of a wide variety of weather and climate extremes (IPCC, 2021), having important impacts on permafrost evolutions (Westermann et al., 2011; Zhu et al., 2017; Jorgenson et al., 2020). Most types of permafrost landscapes have experienced substantial alternations in response to extreme events, such as thaw slumps, icewedge degradation, and ground subsidence (Jorgenson et al., 2020). An isolated or transient extreme could more strongly affect the degradation of permafrost compared to unceasing warming (Marmy et al., 2013). However, the sensitivity of permafrost evolution to different types of extreme events differs between locations and at different stages of soil freezing-thawing processes (Zhu et al., 2017; Jorgenson et al., 2020). For example, summer precipitation events (light, moderate, and heavy) in the TP affect local soil hydrothermal conditions to varying degrees and further contribute to permafrost thawing. Climate extremes (cold, less snowy winters) in the Arctic could cause permafrost aggradation. Compound extreme events, such as heatwaves combined with droughts and compound fire weather conditions (Irannezhad et al., 2020), are projected to occur more frequently in many regions across the globe (IPCC, 2021). The response of permafrost changes in the two regions to the individual or compound extreme events is not yet fully clear and deserves more attention in future research.

8. Summary

Permafrost, a sensitive indicator of climate warming, has undergone dramatic changes in recent decades that are often broadly ascribed to all permafrost regions. This is the first review to comprehensively compare permafrost changes in the Arctic with those on the Third Pole (TP). Large differences in permafrost extent, ground temperatures, active-layer thickness, soil carbon, and environmental characteristics were found between the two regions, causing differing impacts on societal and ecological systems.

The Arctic has experienced more dramatic warming than the TP. Both regions have experienced enhanced warming relative to the global average, caused by polar amplification in the Arctic and elevation-dependent warming on the TP. Under a future warming scenario, the high-latitude permafrost region in the Arctic is expected to experience more rapid warming than the high-altitude permafrost region on the TP. The common main drivers for the warming of the two regions are attributable to snow/ice-albedo feedback and enhanced downward longwave radiation due to increased atmospheric water vapor, but the Arctic is more affected by decreasing sea ice.

Ground temperatures in cold permafrost have increased more rapidly than warm permafrost, probably because latent heat effects retard the rise of permafrost temperature. Consistent with air temperature increases, a greater increase in permafrost temperature has also occurred in the Arctic than on the TP, possibly due to the latent heat effects and moist soil organic matter. Under the RCP scenarios considered, increases in mean annual ground temperature in the Arctic are projected to be faster than those on the TP.

Permafrost extent has generally contracted as temperatures have risen. Near-surface (<10–15 m depth) permafrost area is projected to decline more rapidly on the TP (58%) compared to the Arctic (29%) by 2061–2080, relative to 2000–2014, under the RCP 4.5 climate warming scenario. Few permafrost areas are projected to remain on the TP by 2061–2080 under the RCP 8.5 scenario.

Active-layer thickness in the Arctic (average 100 cm) is generally shallower than on the TP (212 cm). Active-layer thickness varies regionally, and its increase on the TP has been faster than in the Arctic, which is well explained by the larger rise in the warming expressed by the thawing index on the TP. This pattern is projected to continue under different climate scenarios considered.

Permafrost degradation has had tremendous consequences on the socio-economic systems, ecosystems, and hydrological systems over the two polar regions, increasing the geohazard risk. The carbon sink in the ecological systems north of $60^\circ N$ is projected to transform into a CO_2 source by the end of the 21st century, and SOC storage on the TP is expected to decrease significantly.

Degradation of permafrost results in changes in surface energy balance and changes in land-atmosphere interactions. Such changes have caused ongoing environmental deterioration and unpredictable changes to the climate. Land-ocean–atmosphere couplings play crucial roles in the climates over the polar regions, providing possible connections between the two regions that warrant further analysis.

Author contributions

X.W., Y. R., G.P., and B. S. wrote the first draft of the manuscript. X. W., G.P., and Y.R. performed the analyses. X.W. and G.P. drafted the figures. D.C., H.W.C., X.L, M.T.J., J.A., G.D.C., and X.D.W. reviewed and edited the manuscript before submission. R.L. and X.P. provided the permafrost active-layer thickness data. All authors contributed substantially to the discussion of content.

Declaration of Competing Interest

The authors declare that they have no known competing financial interests or personal relationships that could have appeared to influence the work reported in this paper.

Acknowledgments

Special thanks are due to Prof. Frederick Nelson for editing the language and providing some constructive comments for improving the paper. This research was jointly supported by the Strategic Priority Research Program of the Chinese Academy of Sciences (CAS) (XDA19070204, XDA20100102), the National Natural Science Foundation of China (42161025, U21A2006, 41771068), the Second Tibetan Plateau Scientific Expedition and Research Program (STEP) (2019QZKK0208), the Youth Innovation Promotion Association of the CAS (2018460), and the National Key Research and Development Program of China (2020YFA0608501). The authors also acknowledge the China Scholarship Council (201904910442) and Swedish STINT (CH2019-8377, CH2020-8799). This work is a contribution to the Swedish BECC and MERGE. Collaborative support also was provided by the U.S. National Science Foundation (OPP 1820883). We would like to thank the ECMWF data server for providing ERA5 reanalysis data, and the Climate Research Unit (CRU) of University of East Anglia for air temperature and precipitation. Mean annual ground temperature (MAGT) sites in the study selected from the Global Terrestrial Network for Permafrost (GTN-P) is available at https://doi.org/10.1594/PANGA EA.884711. The Circumpolar Active Layer Monitoring (CALM) Program Network is acknowledged for providing the ALT data in the Arctic. The geohazard index can be accessed at https://doi.pangaea.de/10.1594/PA NGAEA.893881.

References

Aalto, J., Karjalainen, O., Hjort, J., Luoto, M., 2018. Statistical forecasting of current and future Circum-Arctic ground temperatures and active layer thickness. Geophys. Res. Lett. 45 (10), 4889–4898.

- Alexandrov, G.A., Ginzburg, V.A., Insarov, G.E., Romanovskaya, A.A., 2021. CMIP6 model projections leave no room for permafrost to persist in Western Siberia under the SSP5-8.5 scenario. Clim. Chang. 169 (3), 42.
- AMAP, 1997. Arctic Pollution Issues: A State of the Arctic Environment Report. Arctic Monitoring and Assessment Programme, p. 188.
- Anthony, K.W., Deimling, T.S.V., Nitze, I., Frolking, S., Emond, A., Daanen, R., Anthony, P., Lindgren, P., Jones, B., Grosse, G., 2018. 21st-century modeled permafrost carbon emissions accelerated by abrupt thaw beneath lakes. Nat. Commun. 9 (1) 3262
- Barrett, D.J., 2002. Steady state turnover time of carbon in the Australian terrestrial biosphere. Glob. Biogeochem. Cycles 16 (4), 1108.
- Baumann, F., He, J.-S., Schmidt, K., Kühn, P., Scholten, T., 2009. Pedogenesis, permafrost, and soil moisture as controlling factors for soil nitrogen and carbon contents across the Tibetan Plateau. Glob. Chang. Biol. 15 (12), 3001–3017.
- Biskaborn, B.K., Smith, S.L., Noetzli, J., Matthes, H., Vieira, G., Streletskiy, D.A., Schoeneich, P., Romanovsky, V.E., Lewkowicz, A.G., Abramov, A., 2019. Permafrost is warming at a global scale. Nat. Commun. 10 (1), 264.
- Blackport, R., Screen, J.A., 2020. Weakened evidence for mid-latitude impacts of Arctic warming. Nat. Clim. Chang. 10 (12), 1065–1066.
- Bonfils, C.J.W., Phillips, T.J., Lawrence, D.M., Cameron-Smith, P., Riley, W.J., Subin, Z. M., 2012. On the influence of shrub height and expansion on northern high latitude climate. Environ. Res. Lett. 7 (1), 015503.
- Bosikov, N., 1998. Wetness variability and dynamics of thermokarst processes in Central Yakutia. In: Proceedings of the 7th International Permafrost Conference, pp. 71–74.
- Box, J.E., Colgan, W.T., Christensen, T.R., Schmidt, N.M., Lund, M., Parmentier, F.-J.W., Brown, R., Bhatt, U.S., Euskirchen, E.S., Romanovsky, V.E., Walsh, J.E., Overland, J. E., Wang, M., Corell, R.W., Meier, W.N., Wouters, B., Mernild, S., Mård, J., Pawlak, J., Olsen, M.S., 2019. Key indicators of Arctic climate change: 1971–2017. Environ. Res. Lett. 14 (4), 045010.
- Brown, J., Ferrians, O., Heginbottom, J.A., Melnikov, E., 2002. Circum-Arctic Map of Permafrost and Ground-Ice Conditions, Version 2. [Indicate Subset Used]. NSIDC: National Snow and Ice Data Center, Boulder, Colorado USA.
- Burke, E.J., Zhang, Y., Krinner, G., 2020. Evaluating permafrost physics in the Coupled Model Intercomparison Project 6 (CMIP6) models and their sensitivity to climate change. Cryosphere 14 (9), 3155–3174.
- Caesar, L., Rahmstorf, S., Robinson, A., Feulner, G., Saba, V., 2018. Observed fingerprint of a weakening Atlantic Ocean overturning circulation. Nature 556 (7700), 191–196.
- Chadburn, S.E., Burke, E.J., Cox, P.M., Friedlingstein, P., Hugelius, G., Westermann, S., 2017. An observation-based constraint on permafrost loss as a function of global warming. Nat. Clim. Chang. 7 (5), 340–344.
- Chapin, F.S., Sturm, M., Serreze, M.C., McFadden, J.P., Key, J.R., Lloyd, A.H., McGuire, A.D., Rupp, T.S., Lynch, A.H., Schimel, J.P., Beringer, J., Chapman, W.L., Epstein, H.E., Euskirchen, E.S., Hinzman, L.D., Jia, G., Ping, C.-L., Tape, K.D., Thompson, C.D.C., Walker, D.A., Welker, J.M., 2005. Role of land-surface changes in Arctic summer warming. Science 310 (5748), 657–660.
- Che, T., Li, X., Jin, R., Armstrong, R., Zhang, T., 2008. Snow depth derived from passive microwave remote-sensing data in China. Ann. Glaciol. 49, 145–154.
- Chen, D., Xu, B., Yao, T., Guo, Z., Cui, P., Chen, F., Zhang, R., Zhang, X., Zhang, Y., Fan, J., Hou, Z., Zhang, T., 2015. Assessment of past, present and future environmental changes on the Tibetan Plateau. Sci. Bull. 60, 3025–3035.
- Chen, H.W., Alley, R.B., Zhang, F., 2016a. Interannual Arctic Sea ice variability and associated winter weather patterns: a regional perspective for 1979–2014. J. Geophys. Res. Atmos. 121 (24), 14433–14455.
- Chen, H.W., Zhang, F., Alley, R.B., 2016b. The robustness of midlatitude weather pattern changes due to Arctic Sea ice loss. J. Clim. 29 (21), 7831–7849.
- Cheng, G., 1979. Some differences in permafrost between Qinghai-Xizang (Tibet) Plateau, China and Canada. J. Glaciol. Geocryol. 1 (2), 39–43 (In Chinese).
- Cheng, G., 1984. Problems on zonation of high-altitude permafrost. Acta Geograph. Sin. 39 (2), 185–193 (In Chinese).
- Cheng, G., Wang, S., 1982. On the zonation of high-altitude permafrost in China. J. Glaciol. Geocryol. 4 (2), 1–17 (In Chinese).
- Cheng, G., Wu, T., 2007. Responses of permafrost to climate change and their environmental significance, Qinghai-Tibet Plateau. J. Geophys. Res. Earth Surf. 112, F02S03.
- Cheng, W., Zhao, S., Zhou, C., Chen, X., 2012. Simulation of the decadal permafrost distribution on the Qinghai-Tibet Plateau (China) over the past 50 years. Permafr. Periglac. Process. 23 (4), 292–300.
- Cheng, G., Zhao, L., Li, R., Wu, X., Sheng, Y., Hu, G., Zou, D., Jin, H., Li, X., Wu, Q., 2019. Characteristic, changes and impacts of permafrost on Qinghai-Tibet Plateau. Chin. Sci. Bull. 64 (0023-074X), 2783.
- Clow, G.D., 2014. Temperature data acquired from the DOI/GTN-P Deep Borehole Array on the Arctic Slope of Alaska, 1973-2013. Earth Syst. Sci. Data 6, 201–218.
- Cohen, J., Screen, J.A., Furtado, J.C., Barlow, M., Whittleston, D., Coumou, D., Francis, J., Dethloff, K., Entekhabi, D., Overland, J., Jones, J., 2014. Recent Arctic amplification and extreme mid-latitude weather. Nat. Geosci. 7, 627.
- Cohen, J., Zhang, X., Francis, J., Jung, T., Kwok, R., Overland, J., Tayler, P., Lee, S., Laliberte, F., Feldstein, S., 2018. Arctic Change and Possible Influence on Mid-Latitude Climate and Weather (US CLIVAR White Paper).
- Cohen, J., Zhang, X., Francis, J., Jung, T., Kwok, R., Overland, J., Ballinger, T.J., et al., 2020. Divergent consensuses on Arctic amplification influence on midlatitude severe winter weather. Nat. Clim. Chang. 10 (1), 20–29.
- Colombo, N., Salerno, F., Gruber, S., Freppaz, M., Williams, M., Fratianni, S., Giardino, M., 2018. Review: Impacts of permafrost degradation on inorganic chemistry of surface fresh water. Glob. Planet. Chang. 162, 69–83.
- Coumou, D., Lehmann, J., Beckmann, J., 2015. The weakening summer circulation in the Northern Hemisphere mid-latitudes. Science 348 (6232), 324–327.

X. Wang et al. Earth-Science Reviews 230 (2022) 104042

Dai, A., Song, M., 2020. Little influence of Arctic amplification on mid-latitude climate. Nat. Clim. Chang. 10 (3), 231–237.

- Delisle, G., 2007. Near-surface permafrost degradation: how severe during the 21st century? Geophys. Res. Lett. 34 (9), L09503.
- Dietz, S., Rising, J., Stoerk, T., Wagner, G., 2021. Economic impacts of tipping points in the climate system. Proc. Natl. Acad. Sci. U. S. A. 118 (34), e2103081118.
- Ding, J., Li, F., Yang, G., Chen, L., Zhang, B., Liu, L., Fang, K., Qin, S., Chen, Y., Peng, Y., Ji, C., He, H., Smith, P., Yang, Y., 2016. The permafrost carbon inventory on the Tibetan Plateau: a new evaluation using deep sediment cores. Glob. Chang. Biol. 22 (8), 2688–2701.
- Ding, Y., Zhang, S., Zhao, L., Li, Z., Kang, S., 2019. Global warming weakening the inherent stability of glaciers and permafrost. Sci. Bull. 64 (4), 245–253.
- Dobinski, W., 2011. Permafrost. Earth-Sci. Rev. 108 (3), 158-169.
- Elberling, B., Michelsen, A., Schädel, C., Schuur, E.A.G., Christiansen, H.H., Berg, L., Tamstorf, M.P., Sigsgaard, C., 2013. Long-term CO2 production following permafrost thaw. Nat. Clim. Chang. 3 (10), 890–894.
- Fick, S.E., Hijmans, R.J., 2017. WorldClim 2: new 1-km spatial resolution climate surfaces for global land areas. Int. J. Climatol. 37 (12), 4302–4315.
- Fisher, J.P., Estop-Aragonés, C., Thierry, A., Charman, D.J., Wolfe, S.A., Hartley, I.P., Murton, J.B., Williams, M., Phoenix, G.K., 2016. The influence of vegetation and soil characteristics on active-layer thickness of permafrost soils in boreal forest. Glob. Chang. Biol. 22 (9), 3127–3140.
- Ford, T.W., Frauenfeld, O.W., 2016. Surface–atmosphere moisture interactions in the frozen ground regions of Eurasia. Sci. Rep. 6 (1), 19163.
- Frauenfeld, O.W., Zhang, T., Mccreight, J.L., 2007. Northern Hemisphere freezing/ thawing index variations over the twentieth century. Int. J. Climatol. 27 (1), 47–63.
- Fu, Y., Ma, Y., Zhong, L., Yang, Y., Guo, X., Wang, C., Xu, X., Yang, K., Xu, X., Liu, L., Fan, G., Li, Y., Wang, D., 2020. Land surface processes and summer cloud-precipitation characteristics in the Tibetan Plateau and their effects on downstream weather: a review and perspective. Natl. Sci. Rev. 7 (3), 500–515.
- Gao, T., Zhang, T., Cao, L., Kang, S., Sillanpää, M., 2016. Reduced winter runoff in a mountainous permafrost region in the northern Tibetan Plateau. Cold Reg. Sci. Technol. 126, 36–43.
- Gao, K., Duan, A., Chen, D., Wu, G., 2019. Surface energy budget diagnosis reveals possible mechanism for the different warming rate among Earth's three poles in recent decades. Sci. Bull. 64 (16), 1140–1143.
- Gao, K., Duan, A., Chen, D., 2020. Interdecadal summer warming of the Tibetan Plateau potentially regulated by a sea surface temperature anomaly in the Labrador Sea. Int. J. Climatol. 1–11.
- Gruber, S., 2012. Derivation and analysis of a high-resolution estimate of global permafrost zonation. Cryosphere 6 (1), 221–233.
- Gruber, S., Fleiner, R., Guegan, E., Panday, P., Schmid, M.O., Stumm, D., Wester, P., Zhang, Y., Zhao, L., 2017. Review article: inferring permafrost and permafrost thaw in the mountains of the Hindu Kush Himalaya region. Cryosphere 11 (1), 81–99.
- Guo, D., Wang, H., 2013. Simulation of permafrost and seasonally frozen ground conditions on the Tibetan Plateau, 1981–2010. J. Geophys. Res. Atmos. 118 (11), 5216–5230.
- Guo, D., Wang, H., 2016. CMIP5 permafrost degradation projection: a comparison among different regions. J. Geophys. Res. Atmos. 121 (9), 4499–4517.
- Guo, D., Li, D., Hua, W., 2018. Quantifying air temperature evolution in the permafrost region from 1901 to 2014. Int. J. Climatol. 38 (1), 66–76.
- Guo, H., Li, X., Qiu, Y., 2020. Comparison of global change at the Earth's three poles using spaceborne Earth observation. Sci. Bull. 65 (16), 1320–1323.
- Heginbottom, J.A., Brown, J., Humlum, O., Svensson, H., 2012. Permafrost and periglacial environments. In: State of the Earth's Cryosphere at the Beginning of the 21st Century: Glaciers, Global Snow Cover, Floating Ice, and Permafrost and Periglacial Environments: Chapter A in Satellite Image Atlas of Glaciers of the World. U.S. Geological Survey, Reston, pp. 425–496.
- Heijmans, M.M.P.D., Magnússon, R.Í., Lara, M.J., Frost, G.V., Myers-Smith, I.H., van Huissteden, J., Jorgenson, M.T., Fedorov, A.N., Epstein, H.E., Lawrence, D.M., Limpens, J., 2022. Tundra vegetation change and impacts on permafrost. Nat. Rev. Earth Environ. 3 (1), 68–84.
- Helbig, M., Wischnewski, K., Kljun, N., Chasmer, L.E., Quinton, W.L., Detto, M., Sonnentag, O., 2016. Regional atmospheric cooling and wetting effect of permafrost thaw-induced boreal forest loss. Glob. Chang. Biol. 22 (12), 4048–4066.
- Hengl, T., Mendes de Jesus, J., Heuvelink, G.B.M., Ruiperez Gonzalez, M., Kilibarda, M., Blagotté, A., Shangguan, W., Wright, M.N., Geng, X., Bauer-Marschallinger, B., Guevara, M.A., Vargas, R., MacMillan, R.A., Batjes, N.H., Leenaars, J.G.B., Ribeiro, E., Wheeler, I., Mantel, S., Kempen, B., 2017. SoilGrids250m: global gridded soil information based on machine learning. PLoS One 12 (2), e0169748.
- Hersbach, H., Bell, B., Berrisford, P., Hirahara, S., Horányi, A., Muñoz-Sabater, J.,
 Nicolas, J., Peubey, C., Radu, R., Schepers, D., Simmons, A., Soci, C., Abdalla, S.,
 Abellan, X., Balsamo, G., Bechtold, P., Biavati, G., Bidlot, J., Bonavita, M., De
 Chiara, G., Dahlgren, P., Dee, D., Diamantakis, M., Dragani, R., Flemming, J.,
 Forbes, R., Fuentes, M., Geer, A., Haimberger, L., Healy, S., Hogan, R.J., Holm, E.,
 Janisková, M., Keeley, S., Laloyaux, P., Lopez, P., Lupu, C., Radnoti, G., de
 Rosnay, P., Rozum, I., Vamborg, F., Villaume, S., Thépaut, J.-N., 2020. The ERA5
 global reanalysis. Q. J. R. Meteorol. Soc. 146 (730), 1999–2049.
- Hinzman, L.D., Kane, D.L., Woo, M.-K., 2005. Permafrost Hydrology. Encyclopedia of Hydrological Sciences.
- Hjort, J., Karjalainen, O., Aalto, J., Westermann, S., Romanovsky, V.E., Nelson, F.E., Etzelmüller, B., Luoto, M., 2018. Degrading permafrost puts Arctic infrastructure at risk by mid-century. Nat. Commun. 9 (1), 5147.
- Hjort, J., Streletskiy, D., Doré, G., Wu, Q., Bjella, K., Luoto, M., 2022. Impacts of permafrost degradation on infrastructure. Nat. Rev. Earth Environ. 3 (1), 24–38.

Honda, M., Inoue, J., Yamane, S., 2009. Influence of low Arctic Sea-ice minima on anomalously cold Eurasian winters. Geophys. Res. Lett. 36 (8), L08707.

- Hong, E., Perkins, R., Trainor, S., 2014. Thaw settlement hazard of permafrost related to climate warming in Alaska. Arctic 67 (1), 93–103.
- Hori, M., Sugiura, K., Kobayashi, K., Aoki, T., Tanikawa, T., Kuchiki, K., Niwano, M., Enomoto, H., 2017. A 38-year (1978–2015) Northern Hemisphere daily snow cover extent product derived using consistent objective criteria from satellite-borne optical sensors. Remote Sens. Environ. 191, 402–418.
- Huang, J., Zhang, X., Zhang, Q., Lin, Y., Hao, M., Luo, Y., Zhao, Z., Yao, Y., Chen, X., Wang, L., Nie, S., Yin, Y., Xu, Y., Zhang, J., 2017. Recently amplified arctic warming has contributed to a continual global warming trend. Nat. Clim. Chang. 7 (12), 875–879.
- Hugelius, G., Strauss, J., Zubrzycki, S., Harden, J.W., Schuur, E., Ping, C.-L., Schirrmeister, L., Grosse, G., Michaelson, G.J., Koven, C.D., 2014. Estimated stocks of circumpolar permafrost carbon with quantified uncertainty ranges and identified data gaps. Biogeosciences (Online) 11 (23), 6573–6593.
- Immerzeel, W.W., Lutz, A., Andrade, M., Bahl, A., Biemans, H., Bolch, T., Hyde, S., Brumby, S., Davies, B., Elmore, A., 2020. Importance and vulnerability of the world's water towers. Nature 577 (7790), 364–369.
- IPCC, 2019. Special Report on the Ocean and Cryosphere in a Changing Climate.
 IPCC, 2021. Summary for policymakers. In: Masson-Delmotte, V., Zhai, P., Pirani, A., Connors, S.L., Péan, C., Berger, S., Caud, N., Chen, Y., Goldfarb, L., Gomis, M.I., Huang, M., Leitzell, K., Lonnoy, E., Matthews, J.B.R., Maycock, T.K., Waterfield, T., Yelekçi, O., Yu, R., Zhou, B. (Eds.), Climate Change 2021: The Physical Science Basis. Contribution of Working Group I to the Sixth Assessment Report of the Intergovernmental Panel on Climate Change. Cambridge University Press (In Press).
- Irannezhad, M., Liu, J., Ahmadi, B., Chen, D., 2020. The dangers of Arctic zombie wildfires. Science 369 (6508), 1171.
- Jeong, J.-H., Kug, J.-S., Kim, B.-M., Min, S.-K., Linderholm, H.W., Ho, C.-H., Rayner, D., Chen, D., Jun, S.-Y., 2012. Greening in the circumpolar high-latitude may amplify warming in the growing season. Clim. Dyn. 38 (7), 1421–1431.
- Jeong, J.-H., Kug, J.-S., Linderholm, H.W., Chen, D., Kim, B.-M., Jun, S.-Y., 2014. Intensified Arctic warming under greenhouse warming by vegetation—atmosphere—sea ice interaction. Environ. Res. Lett. 9 (9), 094007.
- Jiang, H., Yi, Y., Zhang, W., Yang, K., Chen, D., 2020. Sensitivity of soil freeze/thaw dynamics to environmental conditions at different spatial scales in the central Tibetan Plateau. Sci. Total Environ. 734, 139261.
- Jin, H., Luo, D., Wang, S., Lü, L., Wu, J., 2011. Spatiotemporal variability of permafrost degradation on the Qinghai-Tibet Plateau. Sci. Cold Arid Reg. 3 (4), 281–305.
- Jin, H., Jin, X., He, R., Luo, D., Chang, X., Wang, S., Marchenko, S.S., Yang, S., Yi, C., Li, S., Harris, S.A., 2019. Evolution of permafrost in China during the last 20 ka. Sci. China Earth Sci. 62 (8), 1207–1223.
- Jin, X., Jin, H., Iwahana, G., Marchenko, S.S., Luo, D., Li, X., Liang, S., 2021. Impacts of climate-induced permafrost degradation on vegetation: a review. Adv. Clim. Chang. Res. 12 (1), 29–47.
- Jorgenson, M.T., Grosse, G., 2016. Remote sensing of landscape change in permafrost regions. Permafr. Periglac. Process. 27 (4), 324–338.
- Jorgenson, M.T., Racine, C.H., Walters, J.C., Osterkamp, T.E., 2001. Permafrost degradation and ecological changes associated with a warmingclimate in Central Alaska. Clim. Chang. 48 (4), 551–579.
- Jorgenson, M.T., Shur, Y.L., Pullman, E.R., 2006. Abrupt increase in permafrost degradation in Arctic Alaska. Geophys. Res. Lett. 33 (2), L02503.
- Jorgenson, M.T., Romanovsky, V., Harden, J., Shur, Y., O'Donnell, J., Schuur, E.A.G., Kanevskiy, M., Marchenko, S., 2010. Resilience and vulnerability of permafrost to climate change. Can. J. For. Res. 40 (7), 1219–1236.
- Jorgenson, M.T., Harden, J., Kanevskiy, M., O'Donnell, J., Wickland, K., Ewing, S., Manies, K., Zhuang, Q., Shur, Y., Striegl, R., 2013. Reorganization of vegetation, hydrology and soil carbon after permafrost degradation across heterogeneous boreal landscapes. Environ. Res. Lett. 8 (3), 035017.
- Jorgenson, M.T., Kanevskiy, M., Shur, Y., Moskalenko, N., Brown, D.R.N., Wickland, K., Striegl, R., Koch, J., 2015. Role of ground ice dynamics and ecological feedbacks in recent ice wedge degradation and stabilization. J. Geophys. Res. Earth Surf. 120 (11), 2280–2297.
- Jorgenson, M.T., Douglas, T.A., Liljedahl, A.K., Roth, J.E., Cater, T.C., Davis, W.A., et al., 2020. The roles of climate extremes, ecological succession, and hydrology in repeated permafrost aggradation and degradation in fens on the Tanana Flats, Alaska. J. Geophys. Res. Biogeosci. 125 (12) e2020JG005824.
- Kanevskiy, M., Shur, Y., Jorgenson, T., Brown, D.R.N., Moskalenko, N., Brown, J., Walker, D.A., Raynolds, M.K., Buchhorn, M., 2017. Degradation and stabilization of ice wedges: implications for assessing risk of thermokarst in northern Alaska. Geomorphology 297, 20–42.
- Karjalainen, O., Aalto, J., Luoto, M., Westermann, S., Romanovsky, V.E., Nelson, F.E., Etzelmüller, B., Hjort, J., 2019a. Circumpolar permafrost maps and geohazard indices for near-future infrastructure risk assessments. Sci. Data 6, 190037.
- Karjalainen, O., Luoto, M., Aalto, J., Hjort, J., 2019b. New insights into the environmental factors controlling the ground thermal regime across the Northern Hemisphere. Cryosphere 13 (2), 693–707.
- Kokelj, S.V., Jorgenson, M.T., 2013. Advances in thermokarst research. Permafr. Periglac. Process. 24 (2), 108–119.
- Koven, C.D., Ringeval, B., Friedlingstein, P., Ciais, P., Cadule, P., Khvorostyanov, D., Krinner, G., Tarnocai, C., 2011. Permafrost carbon-climate feedbacks accelerate global warming. Proc. Natl. Acad. Sci. U. S. A. 108 (36), 14769–14774.
- Lachenbruch, A.H., Marshall, B.V., 1986. Changing climate: geothermal evidence from permafrost in the Alaskan Arctic. Science 234, 689–696.
- Lachenbruch, A.H., Sass, J.H., Marshall, B.V., Moses, T.H., 1982. Permafrost, heat flow, and the geothermal regime at Prudhoe Bay, Alaska. J. Geophys. Res. 87, 9301–9316.

Earth-Science Reviews 230 (2022) 104042

- Landrum, L., Holland, M.M., 2020. Extremes become routine in an emerging new Arctic. Nat. Clim. Chang. 10 (12), 1108–1115.
- Lantz, T.C., Turner, K.W., 2015. Changes in lake area in response to thermokarst processes and climate in Old Crow Flats, Yukon. J. Geophys. Res. Biogeosci. 120 (3), 513–524.
- Lara, M.J., Genet, H., McGuire, A.D., Euskirchen, E.S., Zhang, Y., Brown, D.R.N., Jorgenson, M.T., Romanovsky, V., Breen, A., Bolton, W.R., 2016. Thermokarst rates intensify due to climate change and forest fragmentation in an Alaskan boreal forest lowland. Glob. Chang. Biol. 22 (2), 816–829.
- Larsen, P.H., Goldsmith, S., Smith, O., Wilson, M.L., Strzepek, K., Chinowsky, P., Saylor, B., 2008. Estimating future costs for Alaska public infrastructure at risk from climate change. Glob. Environ. Chang. 18 (3), 442–457.
- Lawrence, D.M., Slater, A.G., 2010. The contribution of snow condition trends to future ground climate. Clim. Dyn. 34 (7), 969–981.
- Lawrence, D.M., Slater, A.G., Tomas, R.A., Holland, M.M., Deser, C., 2008. Accelerated Arctic land warming and permafrost degradation during rapid sea ice loss. Geophys. Res. Lett. 35 (11), L11506.
- Lawrence, D.M., Slater, A.G., Swenson, S.C., 2012. Simulation of present-day and future permafrost and seasonally frozen ground conditions in CCSM4. J. Clim. 25 (7), 2207–2225
- Legendre, M., Bartoli, J., Shmakova, L., Jeudy, S., Labadie, K., Adrait, A., Lescot, M., Poirot, O., Bertaux, L., Bruley, C., Couté, Y., Rivkina, E., Abergel, C., Claverie, J.-M., 2014. Thirty-thousand-year-old distant relative of giant icosahedral DNA viruses with a pandoravirus morphology. Proc. Natl. Acad. Sci. U. S. A. 111 (11), 4274–4279
- Lenton, T.M., Rockström, J., Gaffney, O., Rahmstorf, S., Richardson, K., Steffen, W., Schellnhuber, H.J., 2019. Climate tipping points—too risky to bet against. Nature 575, 592–595.
- Li, S., Cheng, G., 1996. Map of Permafrost on the Qinghai-Tibet Plateau (1:3,000,000).

 Gansu Culture Press, Lanzhou.
- Li, X., Cheng, G., 1999. A GIS-aided response model of high-altitude permafrost to global change. Sci. China Earth Sci. 42 (1), 72–79.
- Li, R., Zhao, L., Ding, Y., Wu, T., Xiao, Y., Du, E., Liu, G., Qiao, Y., 2012a. Temporal and spatial variations of the active layer along the Qinghai-Tibet Highway in a permafrost region. Chin. Sci. Bull. 57 (35), 4609–4616.
- Li, X., Jin, R., Pan, X., Zhang, T., Guo, J., 2012b. Changes in the near-surface soil freeze-thaw cycle on the Qinghai-Tibetan Plateau. Int. J. Appl. Earth Obs. Geoinf. 17. 33–42.
- Li, R., Gao, Y., Chen, D., Zhang, Y., Li, S., 2018. Contrasting vegetation changes in dry and humid regions of the Tibetan Plateau over recent decades. Sci. Cold Arid Reg. 10 (6), 482–492.
- Li, X., Gou, X., Wang, N., Sheng, Y., Jin, H., Qi, Y., Song, X., Hou, F., Li, Y., Zhao, C., Zou, S., Wang, H., Zheng, D., Chen, Y., Niu, X., 2019. Tightening ecological management facilitates green development in the Qilian Mountains. Chin. Sci. Bull. 64 (27), 2928–2937.
- Li, X., Che, T., Li, X., Wang, L., Duan, A., Shangguan, D., Pan, X., Fang, M., Bao, Q., 2020. CASEarth poles: big data for the three poles. Bull. Am. Meteorol. Soc. 101 (9), F1475–F1491
- Lin, H., Wu, Z., 2011. Contribution of the autumn Tibetan Plateau snow cover to seasonal prediction of North American winter temperature. J. Clim. 24 (11), 2801–2813.
- Linderholm, H.W., Ou, T., Jeong, J.-H., Folland, C.K., Gong, D., Liu, H., Liu, Y., Chen, D., 2011. Interannual teleconnections between the summer North Atlantic Oscillation and the East Asian summer monsoon. J. Geophys. Res. Atmos. 116, D13107.
- Liu, C., Shi, R., Chen, W., 2014a. Eco-regional boundary data of the Roof of the World. Acta Geograph. Sin. 69, 12–19.
- Liu, G., Wu, R., Zhang, Y., Nan, S., 2014b. The summer snow cover anomaly over the Tibetan Plateau and its association with simultaneous precipitation over the mei-yubaiu region. Adv. Atmos. Sci. 31 (4), 755–764.
- Liu, H., Duan, K., Li, M., Shi, P., Yang, J., Zhang, X., Sun, J., 2015. Impact of the North Atlantic Oscillation on the Dipole Oscillation of summer precipitation over the central and eastern Tibetan Plateau. Int. J. Climatol. 35 (15), 4539–4546.
- Liu, S., Wu, Q., Ren, X., Yao, Y., Schroeder, S.R., Hu, H., 2017. Modeled Northern Hemisphere autumn and winter climate responses to realistic Tibetan Plateau and Mongolia snow anomalies. J. Clim. 30 (23), 9435–9454.
- Loranty, M.M., Goetz, S.J., 2012. Shrub expansion and climate feedbacks in Arctic tundra. Environ. Res. Lett. 7 (1), 011005.
- Lund, M., Hansen, B.U., Pedersen, S.H., Stiegler, C., Tamstorf, M.P., 2014. Characteristics of summer-time energy exchange in a high Arctic tundra heath 2000–2010. Tellus Ser. B Chem. Phys. Meteorol. 66 (1), 21631.
- Luo, D., Jin, H., Jin, R., Lin, L., He, R., Chang, X., 2011. The extraction of watershed characteristics of the source area of Yellow River based on SRTM DEM with ArcGIS. In: 2011 International Conference on Remote Sensing, Environ. Transp. Eng. IEEE, pp. 1799–1802.
- Luo, J., Niu, F., Lin, Z., Liu, M., Yin, G., 2015. Thermokarst lake changes between 1969 and 2010 in the Beilu River Basin, Qinghai–Tibet Plateau, China. Sci. Bull. 60 (5), 556–564.
- Luo, D., Wu, Q., Jin, H., Marchenko, S.S., Lü, L., Gao, S., 2016. Recent changes in the active layer thickness across the northern hemisphere. Environ. Earth Sci. 75 (7), 555.
- Marcot, B.G., Jorgenson, M.T., Lawler, J.P., Handel, C.M., DeGange, A.R., 2015.Projected changes in wildlife habitats in Arctic natural areas of Northwest Alaska.Clim. Chang. 130 (2), 145–154.
- Marmy, A., Salzmann, N., Scherler, M., Hauck, C., 2013. Permafrost model sensitivity to seasonal climatic changes and extreme events in mountainous regions. Environ. Res. Lett. 8 (3), 035048.

- McClymont, A.F., Hayashi, M., Bentley, L.R., Christensen, B.S., 2013. Geophysical imaging and thermal modeling of subsurface morphology and thaw evolution of discontinuous permafrost. J. Geophys. Res. Earth Surf. 118 (3), 1826–1837.
- McCusker, K.E., Fyfe, J.C., Sigmond, M., 2016. Twenty-five winters of unexpected Eurasian cooling unlikely due to Arctic Sea-ice loss. Nat. Geosci. 9 (11), 838–842.
- Melnikov, V.P., Pikinerov, P.V., Gennadinik, V.B., Babushkin, A.G., Moskovchenko, D.V., 2019. Change in the hydrological regime of siberian rivers as an indicator of changes in cryological conditions. Dokl. Earth Sci. 487 (2), 990–994.
- Melvin, A.M., Larsen, P., Boehlert, B., Neumann, J.E., Chinowsky, P., Espinet, X., Martinich, J., Baumann, M.S., Rennels, L., Bothner, A., Nicolsky, D.J., Marchenko, S. S., 2017. Climate change damages to Alaska public infrastructure and the economics of proactive adaptation. Proc. Natl. Acad. Sci. U. S. A. 114 (2), E122–E131.
- Miner, K.R., D'Andrilli, J., Mackelprang, R., Edwards, A., Malaska, M.J., Waldrop, M.P., Miller, C.E., 2021. Emergent biogeochemical risks from Arctic permafrost degradation. Nat. Clim. Chang. 11 (10), 809–819.
- Mitchell, T.D., Jones, P.D., 2005. An improved method of constructing a database of monthly climate observations and associated high-resolution grids. Int. J. Climatol. 25 (6), 693–712.
- Mori, M., Watanabe, M., Shiogama, H., Inoue, J., Kimoto, M., 2014. Robust Arctic Sea-ice influence on the frequent Eurasian cold winters in past decades. Nat. Geosci. 7 (12), 869–873.
- Mori, M., Kosaka, Y., Watanabe, M., Nakamura, H., Kimoto, M., 2019. A reconciled estimate of the influence of Arctic Sea-ice loss on recent Eurasian cooling. Nat. Clim. Chang. 9 (2), 123–129.
- Mu, C., Zhang, T., Wu, Q., Peng, X., Cao, B., Zhang, X., Cao, B., Cheng, G., 2015. Editorial: organic carbon pools in permafrost regions on the Qinghai–Xizang (Tibetan) Plateau. Cryosphere 9 (2), 479–486.
- Mu, C., Abbott, B.W., Norris, A.J., Mu, M., Fan, C., Chen, X., Jia, L., Yang, R., Zhang, T., Wang, K., Peng, X., Wu, Q., Guggenberger, G., Wu, X., 2020. The status and stability of permafrost carbon on the Tibetan Plateau. Earth-Sci. Rev. 211, 103433.
- Myers-Smith, I.H., Forbes, B.C., Wilmking, M., Hallinger, M., Lantz, T., Blok, D., Tape, K. D., Macias-Fauria, M., et al., 2011. Shrub expansion in tundra ecosystems: dynamics, impacts and research priorities. Environ. Res. Lett. 6 (4), 045509.
- Natali, S.M., Watts, J.D., Rogers, B.M., Potter, S., Ludwig, S.M., Selbmann, A.-K., Sullivan, P.F., Abbott, B.W., Arndt, K.A., Birch, L., 2019. Large loss of CO2 in winter observed across the northern permafrost region. Nat. Clim. Chang. 9 (11), 852–857.
- Nelson, F.E., Anisimov, O.A., Shiklomanov, N.I., 2001. Subsidence risk from thawing permafrost. Nature 410 (6831), 889–890.
- Nelson, F.E., Anisimov, O.A., Shiklomanov, N.I., 2002. Climate change and hazard zonation in the Circum-Arctic permafrost regions. Nat. Hazards 26 (3), 203–225.
- Ni, J., Wu, T., Zhu, X., Hu, G., Zou, D., Wu, X., Li, R., Xie, C., Qiao, Y., Pang, Q., Hao, J., Yang, C., 2021. Simulation of the present and future projection of permafrost on the Qinghai-Tibet Plateau with statistical and machine learning models. J. Geophys. Res. Atmos. 126 (2) e2020.JD033402.
- Nitze, I., Grosse, G., Jones, B.M., Romanovsky, V.E., Boike, J., 2018. Remote sensing quantifies widespread abundance of permafrost region disturbances across the Arctic and Subarctic. Nat. Commun. 9 (1), 5423.
- Obu, J., 2021. How much of the earth's surface is underlain by permafrost? J. Geophys. Res. Earth Surf. 126 (5) e2021JF006123.
- Obu, J., Westermann, S., Bartsch, A., Berdnikov, N., Christiansen, H.H., Dashtseren, A., Delaloye, R., Elberling, B., Etzelmüller, B., Kholodov, A., 2019. Northern Hemisphere permafrost map based on TTOP modelling for 2000–2016 at 1 km2 scale. Earth-Sci. Rev. 193, 299–316.
- Olsen, M.S., Callaghan, T.V., Reist, J.D., Reiersen, L.O., Dahl-Jensen, D., Granskog, M.A., Goodison, B., Hovelsrud, G.K., Johansson, M., Kallenborn, R., Key, J., Klepikov, A., Meier, W., Overland, J.E., Prowse, T.D., Sharp, M., Vincent, W.F., Walsh, J., 2011. The changing Arctic cryosphere and likely consequences: an overview. Ambio 40 (1), 111–118.
- Overland, J.E., 2016. A difficult Arctic science issue: Midlatitude weather linkages. Polar Sci. 10 (3), 210–216.
- Overland, J.E., Ballinger, T.J., Cohen, J., Francis, J.A., Hanna, E., Jaiser, R., Kim, B.-M., Kim, S.-J., Ukita, J., Vihma, T., Wang, M., Zhang, X., 2021. How do intermittency and simultaneous processes obfuscate the Arctic influence on midlatitude winter extreme weather events? Environ. Res. Lett. 16, 043002.
- Pang, G., Wang, X., Yang, M., 2017. Using the NDVI to identify variations in, and responses of, vegetation to climate change on the Tibetan Plateau from 1982 to 2012. Quat. Int. 444, 87–96.
- Pang, G., Chen, D., Wang, X., Lai, H.-W., 2022. Spatiotemporal variations of land surface albedo and associated influencing factors on the Tibetan Plateau. Sci. Total Environ. 804, 150100.
- Park, H., Kim, Y., Kimball, J.S., 2016. Widespread permafrost vulnerability and soil active layer increases over the high northern latitudes inferred from satellite remote sensing and process model assessments. Remote Sens. Environ. 175, 349–358.
- Pearson, R.G., Phillips, S.J., Loranty, M.M., Beck, P.S.A., Damoulas, T., Knight, S.J., Goetz, S.J., 2013. Shifts in Arctic vegetation and associated feedbacks under climate change. Nat. Clim. Chang. 3 (7), 673–677.
- Peng, X., Zhang, T., Frauenfeld, O.W., Wang, K., Luo, D., Cao, B., Su, H., Jin, H., Wu, Q., 2018. Spatiotemporal changes in active layer thickness under contemporary and projected climate in the Northern Hemisphere. J. Clim. 31 (1), 251–266.
- Pepin, N., Bradley, R.S., Diaz, H.F., Baraer, M., Caceres, E.B., Forsythe, N., Fowler, H., Greenwood, G., Hashmi, M.Z., Liu, X.D., Miller, J.R., Ning, L., Ohmura, A., Palazzi, E., Rangwala, I., Schöner, W., Severskiy, I., Shahgedanova, M., Wang, M.B., Williamson, S.N., Yang, D.Q., 2015. Elevation-dependent warming in mountain regions of the world. Nat. Clim. Chang. 5 (5), 424–430.
- Perlwitz, J., Hoerling, M., Dole, R., 2015. Arctic tropospheric warming: causes and linkages to lower latitudes. J. Clim. 28 (6), 2154–2167.

- Polishchuk, Y.M., Bryksina, N.A., Polishchuk, V.Y., 2015. Remote analysis of changes in the number of small thermokarst lakes and their distribution with respect to their sizes in the cryolithozone of Western Siberia, 2015. IZV. Atmos. Ocean Phy. 51 (9), 999–1006.
- Qian, Q., Jia, X., Wu, R., 2019. Changes in the impact of the autumn Tibet Plateau snow cover on the winter temperature over north america in the mid-1990s. J. Geophys. Res. Atmos. 124 (19), 10321–10343.
- Qin, Y., Wu, T., Zhao, L., Wu, X., Li, R., Xie, C., Pang, Q., Hu, G., Qiao, Y., Zhao, G., 2017.
 Numerical modeling of the active layer thickness and permafrost thermal state across
 Qinghai-Tibetan plateau. J. Geophys. Res. Atmos. 122 (21), 11604–11620.
- Qiu, J., 2012. Thawing permafrost reduces river runoff. Nature. https://www.nature.com/articles/nature.2012.9749.
- Ran, Y., Li, X., Cheng, G., Zhang, T., Wu, Q., Jin, H., Jin, R., 2012. Distribution of permafrost in China: an overview of existing permafrost maps. Permafr. Periglac. Process. 23 (4), 322–333.
- Ran, Y., Li, X., Cheng, G., 2018. Climate warming over the past half century has led to thermal degradation of permafrost on the Qinghai–Tibet Plateau. Cryosphere 12 (2), 595–608
- Ran, Y., Li, X., Cheng, G., Nan, Z., Che, J., Sheng, Y., Wu, Q., Jin, H., Luo, D., Tang, Z., Wu, X., 2021a. Mapping the permafrost stability on the Tibetan Plateau for 2005–2015. Sci. China Earth Sci. 64 (1), 62–79.
- Ran, Y., Jorgenson, M.T., Li, X., Jin, H., Wu, T., Li, R., Cheng, G., 2021b. Biophysical permafrost map indicates ecosystem processes dominate permafrost stability in the Northern Hemisphere. Environ. Res. Lett. 16 (9), 095010.
- Ran, Y., Li, X., Cheng, G., Che, J., Aalto, J., Karjalainen, O., Hjort, J., et al., 2022. New high-resolution estimates of the permafrost thermal state and hydrothermal conditions over the Northern Hemisphere. Earth Syst. Sci. Data 14 (2), 865–884.
- Rangwala, I., Miller, J.R., Xu, M., 2009. Warming in the Tibetan Plateau: possible influences of the changes in surface water vapor. Geophys. Res. Lett. 36 (6).
- Rennermalm, A.K., Wood, E.F., Troy, T.J., 2010. Observed changes in pan-arctic coldseason minimum monthly river discharge. Clim. Dyn. 35 (6), 923–939.
- Revich, B.A., Podolnaya, M.A., 2011. Thawing of permafrost may disturb historic cattle burial grounds in East Siberia. Glob. Health Action 4 (1), 8482.
- Richter-Menge, J., Druckenmiller, M., Andersen, J.K., Andreassen, L.M., Baker, E.H., Ballinger, T.J., Berner, L.T., et al., 2020. The Arctic [in "state of the climate in 2019"]. Bull. Am. Meteorol. Soc. 101 (8), S239–S286.
- Romanovsky, V.E., Smith, S.L., Christiansen, H.H., 2010. Permafrost thermal state in the polar Northern Hemisphere during the international polar year 2007–2009: a synthesis. Permafr. Periglac. Process. 21 (2), 106–116.
- Romanovsky, V., Isaksen, K., Drozdov, D., Anisimov, O., Instanes, A., Leibman, M., McGuire, A.D., Shiklomanov, N., Smith, S., Walker, D., 2017. Changing Permafrost and its Impacts. Snow, Water, Ice and Permafrost in the Arctic (SWIPA) 2017. Arctic Monitoring and Assessment Programme (AMAP), pp. 65–102.
- Rose, A.N., McKee, J.J., Sims, K.M., Bright, E.A., Reith, A.E., Urban, M.L., 2020. LandScan 2019. Oak Ridge National Laboratory, Oak Ridge, TN. https://landscan.ornl.gov/. Accessed 17 December 2021.
- Rowland, J., Jones, C., Altmann, G., Bryan, R., Crosby, B., Hinzman, L., Kane, D., Lawrence, D., Mancino, A., Marsh, P., 2010. Arctic landscapes in transition: responses to thawing permafrost. Eos Trans. AGU 91 (26), 229–230.
- Schaefer, K., Lantuit, H., Romanovsky, V.E., Schuur, E.A.G., Witt, R., 2014. The impact of the permafrost carbon feedback on global climate. Environ. Res. Lett. 9 (8), 085003.
- Schuur, E.A., Mack, M.C., 2018. Ecological response to permafrost thaw and consequences for local and global ecosystem services. Annu. Rev. Ecol. Evol. Syst. 49, 279–301.
- Schuur, E.A.G., Bockheim, J., Canadell, J.G., Euskirchen, E., Field, C.B., Goryachkin, S.
 V., Hagemann, S., Kuhry, P., Lafleur, P.M., Lee, H., Mazhitova, G., Nelson, F.E.,
 Rinke, A., Romanovsky, V.E., Shiklomanov, N., Tarnocai, C., Venevsky, S., Vogel, J.
 G., Zimov, S.A., 2008. Vulnerability of permafrost carbon to climate change:
 implications for the global carbon cycle. BioScience 58 (8), 701–714.
- Schuur, E.A.G., McGuire, A.D., Schädel, C., Grosse, G., Harden, J.W., Hayes, D.J., Hugelius, G., Koven, C.D., Kuhry, P., Lawrence, D.M., Natali, S.M., Olefeldt, D., Romanovsky, V.E., Schaefer, K., Turetsky, M.R., Treat, C.C., Vonk, J.E., 2015. Climate change and the permafrost carbon feedback. Nature 520 (7546), 171–179.
- Screen, J.A., 2017. Simulated atmospheric response to regional and pan-Arctic Sea ice loss. J. Clim. 30 (11), 3945–3962.
- Serreze, M.C., Barry, R.G., 2011. Processes and impacts of Arctic amplification: a research synthesis. Glob. Planet. Chang. 77 (1), 85–96.
- Shen, M., Piao, S., Jeong, S.-J., Zhou, L., Zeng, Z., Ciais, P., Chen, D., Huang, M., Jin, C.-S., Li, L.Z., 2015. Evaporative cooling over the Tibetan Plateau induced by vegetation growth. Proc. Natl. Acad. Sci. U. S. A. 112 (30), 9299–9304.
- Shi, C., Sun, C., Wu, G., Wu, X., Chen, D., Masson-Delmotte, V., Li, J., Xue, J., Li, Z., Ji, D., Zhang, J., Fan, Z., Shen, M., Shu, L., Ciais, P., 2019. Summer temperature over the Tibetan Plateau modulated by Atlantic multidecadal variability. J. Clim. 32 (13), 4055–4067.
- Shur, Y.L., Jorgenson, M.T., 2007. Patterns of permafrost formation and degradation in relation to climate and ecosystems. Permafr. Periglac. Process. 18 (1), 7–19.
- Shur, Y., Hinkel, K.M., Nelson, F.E., 2005. The transient layer: implications for geocryology and climate-change science. Permafr. Periglac. Process. 16 (1), 5–17.
- Slater, A.G., Lawrence, D.M., 2013. Diagnosing present and future permafrost from climate models. J. Clim. 26 (15), 5608–5623.
- Smith, S.L., Wolfe, S.A., Riseborough, D.W., Nixon, F.M., 2009. Active-layer characteristics and summer climatic indices, Mackenzie Valley, Northwest Territories, Canada. Permafr. Periglac. Process. 20 (2), 201–220.
- Smith, S.L., Romanovsky, V.E., Lewkowicz, A.G., Burn, C.R., Allard, M., Clow, G.D., Yoshikawa, K., Throop, J., 2010. Thermal state of permafrost in North America: a

- contribution to the international polar year. Permafr. Periglac. Process. 21 (2), 117-135.
- Song, C., Wang, G., Mao, T., Dai, J., Yang, D., 2019. Linkage between permafrost distribution and river runoff changes across the Arctic and the Tibetan Plateau. Sci. China Earth Sci. 1–11.
- Steffen, W., Richardson, K., Rockström, J., Cornell, S.E., Fetzer, I., Bennett, E.M., Biggs, R., Carpenter, S.R., Vries, W.D., Wit, C.A.D., Folke, C., Gerten, D., Heinke, J., Mace, G.M., Persson, L.M., Ramanathan, V., Reyers, B., Sörlin, S., 2015. Planetary boundaries: Guiding human development on a changing planet. Science 347 (6223), 1259855.
- Streletskiy, D.A., Biskaborn, B., Noetzli, J., Lanckman, J.-P., Romanovsky, V.E., Schoeneich, P., Shiklomanov, N.I., Smith, S.L., Vieira, G., Zhao, L., 2017. Permafrost thermal state [in 'state of the climate in 2016']. Bull. Am. Meteor. Soc. 98, 19–21.
- Streletskiy, D.A., Suter, L.J., Shiklomanov, N.I., Porfiriev, B.N., Eliseev, D.O., 2019. Assessment of climate change impacts on buildings, structures and infrastructure in the Russian regions on permafrost. Environ. Res. Lett. 14 (2), 025003.
- Su, B., Xiao, C., Chen, D., Qin, D., Ding, Y., 2019. Cryosphere services and human well-being. Sustainability 11 (16), 4365.
- Takala, M., Luojus, K., Pulliainen, J., Derksen, C., Lemmetyinen, J., Kärnä, J.-P., Koskinen, J., Bojkov, B., 2011. Estimating northern hemisphere snow water equivalent for climate research through assimilation of space-borne radiometer data and ground-based measurements. Remote Sens. Environ. 115 (12), 3517–3529.
- Tape, K., Sturm, M., Racine, C., 2006. The evidence for shrub expansion in Northern Alaska and the Pan-Arctic. Glob. Chang. Biol. 12 (4), 686–702.
- Tarnocai, C., Canadell, J.G., Schuur, E.A.G., Kuhry, P., Mazhitova, G., Zimov, S., 2009. Soil organic carbon pools in the northern circumpolar permafrost region. Glob. Biogeochem. Cycles 23 (2), GB2023.
- Teufel, B., Sushama, L., 2019. Abrupt changes across the Arctic permafrost region endanger northern development. Nat. Clim. Chang. 9 (11), 858–862.
- Tumpey, T.M., Basler, C.F., Aguilar, P.V., Zeng, H., Solórzano, A., Swayne, D.E., Cox, N. J., Katz, J.M., Taubenberger, J.K., Palese, P., García-Sastre, A., 2005. Characterization of the reconstructed 1918 Spanish Influenza pandemic virus. Science 310 (5745), 77–80.
- Turner, A.K., Schuster, R.L., 1996. Landslides: Investigation and mitigation. In: Special Report 247. Trans. Res. Board. National Academy Press, Washington, DC, p. 678.
- van den Hoogen, J., Geisen, S., Routh, D., Ferris, H., Traunspurger, W., Wardle, D.A., et al., 2019. Soil nematode abundance and functional group composition at a global scale. Nature 572 (7768), 194–198.
- Viovy, N.C., 2018. CRUNCEP Data Set. https://vesg.ipsl.upmc.fr/thredds/catalog/work/p529viov/cruncep/V8_1901_2016/catalog.html.
- Vonk, J.E., Tank, S.E., Bowden, W.B., Laurion, I., Vincent, W.F., Alekseychik, P., Amyot, M., Billet, M., Canario, J., Cory, R.M., 2015. Reviews and syntheses: effects of permafrost thaw on Arctic aquatic ecosystems. Biogeosciences 12 (23), 7129–7167.
- Walker, D.A., Raynolds, M.K., Daniëls, F.J., Einarsson, E., Elvebakk, A., Gould, W.A., Katenin, A.E., Kholod, S.S., Markon, C.J., Melnikov, E.S., 2005. The circumpolar Arctic vegetation map. J. Veg. Sci. 16 (3), 267–282.
- Walsh, M.G., de Smalen, A.W., Mor, S.M., 2018. Climatic influence on anthrax suitability in warming northern latitudes. Sci. Rep. 8 (1), 9269.
- Walvoord, M.A., Kurylyk, B.L., 2016. Hydrologic impacts of thawing permafrost—A review. Vadose Zone J. 15 (6), 1–20.
- Wang, B., French, H.M., 1995. Permafrost on the Tibet Plateau, China. Quat. Sci. Rev. 14 (3), 255–274.
- Wang, G., Hu, H., Li, T., 2009. The influence of freeze-thaw cycles of active soil layer on surface runoff in a permafrost watershed. J. Hydrol. 375 (3), 438–449.
- Wang, G., Liu, G., Li, C., Yang, Y., 2012. The variability of soil thermal and hydrological dynamics with vegetation cover in a permafrost region. Agric. For. Meteorol. 162-163, 44-57
- Wang, X., Pang, G., Yang, M., Wan, G., 2016. Effects of modified soil water-heat physics on RegCM4 simulations of climate over the Tibetan Plateau. J. Geophys. Res. Atmos. 121 (12), 6692–6712.
- Wang, K., Zhang, T., Zhang, X., Clow, G.D., Jafarov, E.E., Overeem, I., Romanovsky, V., Peng, X., Cao, B., 2017. Continuously amplified warming in the Alaskan Arctic: implications for estimating global warming hiatus. Geophys. Res. Lett. 44 (17), 9029–9038.
- Wang, X., Pang, G., Yang, M., 2018a. Precipitation over the Tibetan Plateau during recent decades: a review based on observations and simulations. Int. J. Climatol. 38 (3), 1116–1131.
- Wang, S., Sheng, Y., Li, J., Wu, J., Cao, W., Ma, S., 2018b. An estimation of ground ice volumes in permafrost layers in northeastern Qinghai-Tibet Plateau, China. Chin. Geogr. Sci. 28 (1), 61–73.
- Wang, X., Pang, G., Yang, M., Wan, G., Liu, Z., 2018c. Precipitation changes in the Qilian Mountains associated with the shifts of regional atmospheric water vapour during 1960–2014. Int. J. Climatol. 38 (12), 4355–4368.
- Wang, T., Yang, D., Yang, Y., Piao, S., Li, X., Cheng, G., Fu, B., 2020. Permafrost thawing puts the frozen carbon at risk over the Tibetan Plateau. Sci. Adv. 6 (19), eaaz3513.
- Wang, L., Yao, T., Chai, C., Cuo, L., Su, F., Zhang, F., Yao, Z., Zhang, Y., Li, X., Qi, J., Hu, Z., Liu, J., Wang, Y., 2021a. TP-river: monitoring and quantifying total river runoff from the Third Pole. Bull. Am. Meteorol. Soc. 102 (5), E948–E965.
- Wang, P., Huang, Q., Pozdniakov, S.P., Liu, S., Ma, N., Wang, T., Zhang, Y., Yu, J., Xie, J., Fu, G., Frolova, N.L., Liu, C., 2021b. Potential role of permafrost thaw on increasing Siberian river discharge. Environ. Res. Lett. 16 (3), 034046.
- Westermann, S., Boike, J., Langer, M., Schuler, T.V., Etzelmüller, B., 2011. Modeling the impact of wintertime rain events on the thermal regime of permafrost. Cryosphere 5 (4), 945–959.

- Winterfeld, M., Mollenhauer, G., Dummann, W., Köhler, P., Lembke-Jene, L., Meyer, V. D., Hefter, J., McIntyre, C., Wacker, L., Kokfelt, U., Tiedemann, R., 2018. Deglacial mobilization of pre-aged terrestrial carbon from degrading permafrost. Nat. Commun. 9 (1), 3666.
- Wu, Q., Zhang, T., 2008. Recent permafrost warming on the Qinghai-Tibetan Plateau. J. Geophys. Res. Atmos. 113 (D13), D13108.
- Wu, Q., Zhang, T., 2010. Changes in active layer thickness over the Qinghai-Tibetan Plateau from 1995 to 2007. J. Geophys. Res. Atmos. 115 (D9), D09107.
- Wu, J., Sheng, Y., Wu, Q., Wen, Z., 2010. Processes and modes of permafrost degradation on the Qinghai-Tibet Plateau. Sci. China Earth Sci. 53 (1), 150–158.
- Wu, Q., Zhang, T., Liu, Y., 2012a. Thermal state of the active layer and permafrost along the Qinghai-Xizang (Tibet) Railway from 2006 to 2010. Cryosphere 6, 607–612.
- Wu, Z., Li, J., Jiang, Z., Ma, T., 2012b. Modulation of the Tibetan Plateau snow cover on the ENSO teleconnections: from the East Asian summer monsoon perspective. J. Clim. 25 (7), 2481–2489.
- Wu, G., Duan, A., Liu, Y., Mao, J., Ren, R., Bao, Q., He, B., Liu, B., Hu, W., 2014. Tibetan Plateau climate dynamics: recent research progress and outlook. Natl. Sci. Rev. 2 (1), 100–116.
- Wu, Z., Boke-Olén, N., Fensholt, R., Ardö, J., Eklundh, L., Lehsten, V., 2018. Effect of climate dataset selection on simulations of terrestrial GPP: highest uncertainty for tropical regions. PLoS One 13 (6), e0199383.
- Wu, D., Liu, D., Wang, T., Ding, J., He, Y., Ciais, P., Zhang, G., Piao, S., 2021. Carbon turnover times shape topsoil carbon difference between Tibetan Plateau and Arctic tundra. Sci. Bull. 66 (16), 1698–1704.
- Xiao, Z., Liang, S., Wang, J., Chen, P., Yin, X., Zhang, L., Song, J., 2014. Use of general regression neural networks for generating the GLASS leaf area index product from time-series MODIS surface reflectance. IEEE Trans. Geosci. Remote Sens. 52 (1), 200–223
- Xu, X., Sun, C., Chen, D., Zhao, T., Xu, J., Zhang, S., Li, J., Chen, B., Zhao, Y., Dong, L., Sun, X., Zhu, Y., 2021. A vertical transport window of water vapor in the troposphere over the Tibetan Plateau with implication for global change. Atmos. Chem. Phys. Discuss. 2021, 1–20.
- Yang, K., Wang, C., 2019. Seasonal persistence of soil moisture anomalies related to freeze-thaw over the Tibetan Plateau and prediction signal of summer precipitation in eastern China. Clim. Dyn. 53 (3), 2411–2424.
- Yang, Y., Fang, J., Tang, Y., Ji, C., Zheng, C., He, J., Zhu, B., 2008. Storage, patterns and controls of soil organic carbon in the Tibetan grasslands. Glob. Chang. Biol. 14 (7), 1592–1599.
- Yang, M., Nelson, F.E., Shiklomanov, N.I., Guo, D., Wan, G., 2010. Permafrost degradation and its environmental effects on the Tibetan Plateau: a review of recent research. Farth-Sci. Rev. 103, 31–44.
- Yang, Y., Hopping, K.A., Wang, G., Chen, J., Peng, A., Klein, J.A., 2018. Permafrost and drought regulate vulnerability of Tibetan Plateau grasslands to warming. Ecosphere 9 (5), e02233.
- Yang, M., Wang, X., Pang, G., Wan, G., Liu, Z., 2019. The Tibetan Plateau cryosphere: observations and model simulations for current status and recent changes. Earth-Sci. Rev. 190, 353–369.
- Yao, T., Xue, Y., Chen, D., Chen, F., Thompson, L., Cui, P., Koike, T., Lau, W.K.-M., Lettenmaier, D., Mosbrugger, V., Zhang, R., et al., 2019. Recent Third Pole's rapid warming accompanies cryospheric melt and water cycle intensification and interactions between monsoon and environment: multidisciplinary approach with observations, modeling, and analysis. Bull. Am. Meteorol. Soc. 100 (3), 423–444.
- Yi, Y., Kimball, J.S., Chen, R.H., Moghaddam, M., Reichle, R.H., Mishra, U., Zona, D., Oechel, W.C., 2018. Characterizing permafrost active layer dynamics and sensitivity to landscape spatial heterogeneity in Alaska. Cryosphere 12 (1), 145–161.
- You, Q., Chen, D., Wu, F., Pepin, N., Cai, Z., Ahrens, B., Jiang, Z., Wu, Z., Kang, S., AghaKouchak, A., 2020. Elevation dependent warming over the Tibetan Plateau: patterns, mechanisms and perspectives. Earth-Sci. Rev. 210, 103349.
- You, Q., Cai, Z., Pepin, N., Chen, D., Ahrens, B., Jiang, Z., Wu, F., Kang, S., Zhang, R., Wu, T., Wang, P., Li, M., Zuo, Z., Gao, Y., Zhai, P., Zhang, Y., 2021. Warming amplification over the Arctic Pole and Third Pole: trends, mechanisms and consequences. Earth-Sci. Rev. 217, 103625.

- Yun, H., Tang, J., D'Imperio, L., Wang, X., Qu, Y., Liu, L., Zhuang, Q., Zhang, W., Wu, Q., Chen, A., Zhu, Q., Chen, D., Elberling, B., 2022. Warming and increased respiration have transformed an alpine steppe ecosystem on the Tibetan Plateau from a carbon dioxide sink into a source. J. Geophys. Res. Biogeosci. 127 (1) e2021JG006406.
- Zerefos, C.S., Solomos, S., Kapsomenakis, J., Poupkou, A., Dimitriadou, L., Polychroni, I. D., Kalabokas, P., Philandras, C.M., Thanos, D., 2020. Lessons learned and questions raised during and post-COVID-19 anthropopause period in relation to the environment and climate. Environ. Dev. Sustain. 1–23.
- Zhang, T., Barry, R.G., Knowles, K., Heginbottom, J., Brown, J., 1999. Statistics and characteristics of permafrost and ground-ice distribution in the Northern Hemisphere. Polar Geogr. 23 (2), 132–154.
- Zhang, T., Heginbottom, J.A., Barry, R.G., Brown, J., 2000. Further statistics on the distribution of permafrost and ground ice in the Northern Hemisphere. Polar Geogr. 24 (2), 126–131.
- Zhang, K., Kimball, J.S., Kim, Y., McDonald, K.C., 2011. Changing freeze-thaw seasons in northern high latitudes and associated influences on evapotranspiration. Hydrol. Process. 25 (26), 4142–4151.
- Zhang, X., He, J., Zhang, J., Polyakov, I., Gerdes, R., Inoue, J., Wu, P., 2013. Enhanced poleward moisture transport and amplified northern high-latitude wetting trend. Nat. Clim. Chang. 3, 47–51.
- Zhang, G., Yao, T., Shum, C.K., Yi, S., Yang, K., Xie, H., Feng, W., Bolch, T., Wang, L., Behrangi, A., Zhang, H., Wang, W., Xiang, Y., Yu, J., 2017. Lake volume and groundwater storage variations in Tibetan Plateau's endorheic basin. Geophys. Res. Lett. 44 (11), 5550–5560.
- Zhang, Y., Zou, T., Xue, Y., 2019. An Arctic-Tibetan connection on subseasonal to seasonal time scale. Geophys. Res. Lett. 46 (5), 2790–2799.
- Zhang, Z., Wu, Q., Jiang, G., Gao, S., Chen, J., Liu, Y., 2020. Changes in the permafrost temperatures from 2003 to 2015 in the Qinghai-Tibet Plateau. Cold Reg. Sci. Technol. 169, 102904.
- Zhang, G., Nan, Z., Zhao, L., Liang, Y., Cheng, G., 2021. Qinghai-Tibet Plateau wetting reduces permafrost thermal responses to climate warming. Earth Planet. Sci. Lett. 562, 116858.
- Zhao, L., Wu, Q., Marchenko, S.S., Sharkhuu, N., 2010. Thermal state of permafrost and active layer in Central Asia during the international polar year. Permafr. Periglac. Process. 21 (2), 198–207.
- Zhao, L., Hu, G., Zou, D., Wu, X., Ma, L., Sun, Z., Yuan, L., Zhou, H., Liu, S., 2019.
 Permafrost changes and its effects on hydrological processes on Qinghai-Tibet Plateau. Bull. Chin. Acad. Sci. 34 (11), 1233–1246.
- Zhao, L., Zou, D., Hu, G., Du, E., Pang, Q., Xiao, Y., Li, R., Sheng, Y., Wu, X., Sun, Z., Wang, L., Wang, C., Ma, L., Zhou, H., Liu, S., 2020. Changing climate and the permafrost environment on the Qinghai–Tibet (Xizang) plateau. Permafr. Periglac. Process. 31 (3), 396–405.
- Zhao, L., Zou, D., Hu, G., Wu, T., Du, E., Liu, G., Xiao, Y., Li, R., Pang, Q., Qiao, Y., Wu, X., Sun, Z., Xing, Z., Sheng, Y., Zhao, Y., Shi, J., Xie, C., Wang, L., Wang, C., Cheng, G., 2021. A synthesis dataset of permafrost thermal state for the Qinghai–Tibet (Xizang) Plateau, China. Earth Syst. Sci. Data 13 (8), 4207–4218.
- Zhou, Y., Guo, D., Qiu, G., Cheng, G., Li, S., 2000. Geocryology in China. Chinese Academy of Sciences, Beijing (in Chinese).
- Zhu, Y., Liu, H., Ding, Y., Zhang, F., Li, W., 2015. Interdecadal variation of spring snow depth over the Tibetan Plateau and its influence on summer rainfall over East China in the recent 30 years. Int. J. Climatol. 35 (12), 3654–3660.
- Zhu, X., Wu, T., Li, R., Xie, C., Hu, G., Qin, Y., Wang, W., Hao, J., Yang, S., Ni, J., Yang, C., 2017. Impacts of summer extreme precipitation events on the hydrothermal dynamics of the active layer in the Tanggula permafrost region on the Qinghai-Tibetan Plateau. J. Geophys. Res. Atmos. 122 (21), 11549–11567.
- Zhu, D., Ciais, P., Krinner, G., Maignan, F., Jornet Puig, A., Hugelius, G., 2019. Controls of soil organic matter on soil thermal dynamics in the northern high latitudes. Nat. Commun. 10 (1), 3172.
- Zou, D., Zhao, L., Sheng, Y., Chen, J., Hu, G., Wu, T., Wu, J., Xie, C., Wu, X., Pang, Q., Wang, W., Du, E., Li, W., Liu, G., Li, J., Qin, Y., Qiao, Y., Wang, Z., Shi, J., Cheng, G., 2017. A new map of permafrost distribution on the Tibetan Plateau. Cryosphere 11 (6), 2527–2542.